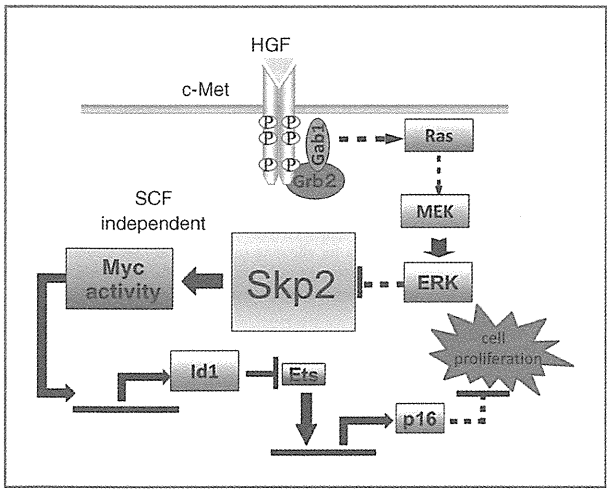

Figure 7. Schematic model of the involvement of Skp2 downregulation in the HGF-induced inhibition of cell proliferation. HGF treatment of the cells downregulates Skp2 expression in an ERK-dependent manner, leading to a reduction in Myc activity. The reduction in Myc activity induces a decrease in Id1, which leads to the activation of a transcription factor, Ets. The activated Ets upregulates p16 expression, which eventually induces inhibition of proliferation in HepG2 hepatoma cells.

involvement of the downregulation of Skp2 in the inhibition of the cell proliferation by HGF. Treatment with HGF downregulates Skp2 expression in an ERK-dependent manner, leading to reduced transcriptional activity of Myc. The reduction in Myc activity decreases Id1 expression, which leads to the activation of a transcription factor, Ets. The activated Ets upregulates p16 expression, which results in inhibition of proliferation in HepG2 hepatoma cells. However, the detailed mechanism of how Skp2 affects Myc activity remains to be elucidated. As Myc activity is generally regulated in the balance of Myc/Max/Mad complexes, we conducted immunoprecipitation assays to analyze the Myc/Max complex, which is the transcription-active form, in the absence or presence of HGF. We found that the amount of Myc/Max complex is not altered even in the presence of HGF (Supplementary Fig. S9), suggesting that Skp2 affects Myc activity not through disruption of the balance of the complexes.

It was previously reported that Skp2 activates the transcription factor c-Myc via ubiquitination as a component of SCF^{Skp2}, which leads to the upregulation of a subset of target genes involved in cell proliferation (18, 19). In contrast, a recent report showed that ubiquitination of c-Myc by the SCF complex is not involved in Myc's activation by Skp2, and this activation upregulates a target gene, *RhoA*, in cell invasion, through a novel transcription complex consisting of Myc-Skp2-Miz1-p300 (20). In the present study, our data suggested that Skp2 functions as a transcriptional activator of Myc rather than a component of the SCF complex in HGF signaling in HepG2 cells (Fig. 5). Thus, in addition to the upregulation of RhoA in cell invasion, it is possible that the Myc-Skp2-Miz1-p300 transcription complex is involved in the regulation of cell proliferation through upregulation of Id1 expression.

We showed that Skp2 is downregulated at the mRNA level in an ERK-dependent manner in HepG2 cells treated with HGF (Fig. 1). Previous reports showed that transcription factor E2F regulates Skp2 expression at the mRNA level in an Akt-dependent manner in other types of cells (34). Although it was previously shown that the inhibitory effect of HGF on the proliferation of HepG2 cells is independent of Akt signaling (7), E2F seemed to be a candidate transcription factor responsible for the Skp2 expression in HGF signaling, because we found that HGF treatment of HepG2 cells reduces the levels of E2F1, and E2F activity (data not shown). To address whether E2F regulates Skp2 expression in HGF signaling, we constructed another HepG2 cell line, in which E2F1 is induced by addition of IPTG. Induction of E2F1 was successfully activated an E2F-responsive promoter, but had no effect on Skp2 expression (data not shown). This result indicated that the regulatory mechanism of Skp2 downregulation induced by HGF is different from that in Akt signaling.

It is generally recognized that the amount of p27 protein, which is predominantly regulated by degradation through ubiquitination by SCF^{Skp2}, is responsible for the suppression of cell proliferation (14). The effect of p27 on the proliferation of HepG2 cells was shown in a previous report, in which β1-integrin–mediated downregulation of p27 through upregulation of Skp2 accelerated the proliferation (26). As HGF treatment of HepG2 cells upregulates p27 protein, we had expected the upregulation to contribute to the suppression of cell proliferation by HGF. However, in the present study, our data showed that partial inhibition of the strong ERK activation, which restores both the amount of Skp2 and cell proliferation suppressed by HGF, has no effect on the upregulation of p27 induced with HGF (Fig. 1B). Our data also showed that high expression of Skp2 restores the cell proliferation suppressed by HGF without affecting the upregulation of p27 (Fig. 2). These results indicate that the upregulation of p27 does not contribute to the suppression of HepG2 cell proliferation by HGF. Accumulating data suggest that p27 has another role in regulating cell motility and migration independent of its cell-cycle role. p27 increases the stability of actin stress fibers by binding to and inhibiting RhoA in cytoplasm, which results in an increase in cell motility (35). As HGF treatment increases the motility of HepG2 cells, leading to cell scattering, the upregulation of p27 might contribute to the increased cell motility with HGF. The significance of the upregulation of p27 expression in HepG2 cells treated with HGF remains to be elucidated.

It was previously shown that the overexpression of Myc in the liver induces the formation of hepatocellular tumors (36, 37), and its inactivation results in regression of the tumors and differentiation of the tumor cells into normal liver cells such as hepatocytes (21), indicating the importance of Myc activity for hepatocarcinogenesis. Accumulating evidence also indicates an important role for Myc activation in the progression of hepatomas (22, 38, 39). We showed here that endogenous Myc activity is regulated by Skp2 in a hepatoma cell line. Thus, it is likely that Skp2 has an important role in

hepatocarcinoma through the regulation of Myc activity. Another report suggested suppression of Myc-induced hepatocarcinogenesis by HGF: hepatocarcinogenesis was induced in transgenic mice expressing c-Myc, but not in transgenic mice expressing c-Myc in combination with HGF (40). The suppression might be caused by downregulation of Skp2. While we showed that HGF treatments of two hepatoma cell lines, HepG2 and HuH7, downregulate Skp2 mRNA in the presence of HGF, further studies of Skp2 in liver tumors and other hepatoma cells would be required to elucidate the involvement of Skp2 in Myc-induced hepatocarcinogenesis, and its suppression via downregulation of Skp2.

Disclosure of Potential Conflicts of Interest

No potential conflicts of interest were disclosed.

Authors' Contributions

Conception and design: T. Tanaka
Development of methodology: Y. Inagaki
Acquisition of data (provided animals, acquired and managed patients, provided facilities, etc.): X. Li, Y. Takizawa, T. Hashimoto, Y. Inagaki, M. Komada, T. Tanaka
Analysis and interpretation of data (e.g., statistical analysis, biostatistics, computational analysis): X. Li, Y. Bian, T. Tanaka
Writing, review, and/or revision of the manuscript: M. Komada, T. Tanaka
Administrative, technical, or material support (i.e., reporting or organizing data, constructing databases): T. Tanaka
Study supervision: T. Ikoma, J. Tanaka, N. Kitamura, M. Komada, T. Tanaka

Acknowledgments

The authors thank Dr. Eiji Hara for allowing us to use the -247 promoter. The authors also thank Mr. Takahito Nakayama and Ms. Hiroko Shirai for supporting our experiments and for information on the Id1 promoter, respectively.

Grant Support

This work was supported by Grants-in-aid for Scientific Research (No. 19570124 and No. 22570137; to T.Tanaka, No. 24241044; to T.Ikoma) from the Japan Society for the Promotion of Science.

The costs of publication of this article were defrayed in part by the payment of page charges. This article must therefore be hereby marked *advertisement* in accordance with 18 U.S.C. Section 1734 solely to indicate this fact.

Received December 29, 2012; revised May 1, 2013; accepted May 17, 2013; published OnlineFirst October 30, 2013.

References

1. Zarnegar R, Michalopoulos GK. The many faces of hepatocyte growth factor: from hepatopoiesis to hematopoiesis. J Cell Biol 1995;129:1177–80.
2. Ma PC, Maulik G, Christensen J, Salgia R. c-Met: structure, functions and potential for therapeutic inhibition. Cancer Metast Rev 2003;22:309–25.
3. Tajima H, Matsumoto K, Nakamura T. Hepatocyte growth factor has potent anti-proliferative activity in various tumor cell lines. FEBS Lett 1991;291:229–32.
4. Shiota G, Rhoads DB, Wang TC, Nakamura T, Schmidt EV. Hepatocyte growth factor inhibits growth of hepatocellular carcinoma cells. Proc Natl Acad Sci U S A 1992;89:373–7.
5. Furge KA, Zhang Y-W, Vande Woude GF. Met receptor tyrosine kinase: enhanced signaling through adapter proteins. Oncogene 2000;19:5582–9.
6. Nakanishi K, Fujimoto J, Ueki T, Kishimoto K, Hashimoto-Tamaoki T, Furuyama J, et al. Hepatocyte growth factor promotes migration of human hepatocellular carcinoma via phosphatidylinositol 3-kinase. Clin Exp Metastas 1999;17:507–14.
7. Tsukada Y, Miyazawa K, Kitamura N. High intensity ERK signal mediates hepatocyte growth factor-induced proliferation inhibition of the human hepatocellular carcinoma cell line HepG2. J Biol Chem 2001;276:40968–76.
8. Tsukada Y, Tanaka T, Miyazawa K, Kitamura N. Involvement of down-regulation of Cdk2 activity in hepatocyte growth factor-induced cell cycle arrest at G1 in the human hepatocellular carcinoma cell line HepG2. J Biochem 2004;136:701–9.
9. Han J, Tsukada Y, Hara E, Kitamura N, Tanaka T. Hepatocyte growth factor induces redistribution of p21(CIP1) and p27(KIP1) through ERK-dependent p16(INK4a) up-regulation, leading to cell cycle arrest at G1 in HepG2 hepatoma cells. J Biol Chem 2005;280:31548–56.
10. Ushio K, Hashimoto T, Kitamura N, Tanaka T. Id1 is down-regulated by hepatocyte growth factor via ERK-dependent and ERK-independent signaling pathways, leading to increased expression of $p16^{Ink4a}$ in hepatoma cells. Mol Cancer Res 2009;7:1179–88.
11. Zheng N, Schulman BA, Song L, Miller JJ, Jeffrey PD, Wang P, et al. Structure of the Cul1-Rbx1-Skp1-F boxSkp2 SCF ubiquitin ligase complex. Nature 2002;416:703–9.
12. Frescas D, Pagano M. Deregulated proteolysis by the F-box proteins Skp2 and beta-TrCP: tipping the scales of cancer. Nat Rev Cancer 2008;8:438–49.
13. Carrano AC, Eytan E, Hershko A, Pagano M. Skp2 is required for the ubiquitin-mediated degradation of the Cdk-inhibitor p27. Nat Cell Biol 1999;1:193–9.
14. Sutterluty H, Chatelain E, Marti A, Wirbelauer C, Senften M, Müller U, et al. p45/Skp2 promotes p27/Kip1 degradation and induces S phase in quiescent cells. Nat Cell Biol 1999;1:207–14.
15. Gstaiger M, Jordan R, Lim M, Catzavelos C, Mestan J, Slinger-land J, et al. Skp2 is oncogenic and overexpressed in human cancers. Proc Natl Acad Sci U S A 2001;98:5043–8.
16. Latres E, Chiarle R, Schulman BA, Pavletich NP, Pellicer A, Inghirami G, et al. Role of the F-box protein Skp2 in lymphomagenesis. Proc Natl Acad Sci U S A 2001;98:2515–20.
17. Oliveira AA, Okuno SH, Nascimento AG, Lloyd RV. Skp2 protein expression in soft tissue sarcomas. J Clin Oncol 2003;21:722–7.
18. Kim SY, Herbst A, Tworkowski KA, Salghetti SE, Tansey WP. Skp2 regulates Myc protein stability and activity. Mol Cell 2003;11:1177–88.
19. von der Lehr N, Johansson S, Wu S, Bahram F, Castell A, Cetinkaya C, et al. The F-box protein Skp2 participates in c-Myc proteosomal degradation and acts as a cofactor for c-Myc-regulated transcription. Mol Cell 2003;11:1189–200.
20. Chan CH, Lee SW, Li CF, Wang J, Yang WL, Wu CY, et al. Deciphering the transcriptional complex critical for RhoA gene expression and cancer metastasis. Nat Cell Biol 2010;12:457–67.
21. Shachaf CM, Kopelman AM, Arvanitis C, Karlsson A, Beer S, Mandl S, et al. Myc inactivation uncovers pluripotent differentiation and tumour dormancy in hepatocellular cancer. Nature 2004;431:1112–7.
22. Kaposi-Novak P, Libbrecht L, Woo HG, Lee YH, Sears NC, Coulouarn C, et al. Central role of c-Myc during malignant conversion in human hepatocarcinogenesis. Cancer Res 2009;69:2775–82.
23. Tanaka T, Kubota M, Shinohara K, Yasuda K, Kato J-Y. *In vivo* analysis of the cyclin D1 promoter during early embryogenesis in *Xenopus*. Cell Stuct Funct 2003;28:165–77.
24. Shirako E, Hirayama N, Tsukada Y, Tanaka T, Kitamura N. Up-regulation of $p21^{CIP1}$ expression mediated by ERK-dependent and –independent pathways contributes to hepatocyte growth factor induced inhibition of HepG2 hepatoma cell proliferation. J Cell Biochem 2008;104:176–88.
25. Kondo A, Hirayama N, Sugito Y, Shono M, Tanaka T, Kitamura N. Coupling of Grb2 to Gab1 mediates hepatocyte growth factor-induced high Intensity ERK signalrequired for inhibition of HepG2 hepatoma cell proliferation. J Biol Chem 2008;283:1428–36.
26. Zhang H, Ozaki I, Mizuta T, Yoshimura T, Matsuhashi S, Hisatomi A, et al. Mechanism of beta 1-integrin-mediated hepatoma cell growth

involves p27 and S-phase kinase-associated protein 2. Hepatology 2003;38:305–13.
27. Zhao Y, Jian W, Gao W, Zheng YX, Wang YK, Zhou ZQ, et al. RNAi silencing of c-Myc inhibits cell migration, invasion, and proliferation in $HepG_2$ human hepatocellular carcinoma cell line: c-Myc silencing in hepatocellular carcinoma cell. Cancer Cell Int 2013;13:23.
28. Hann SR, Eisenman RN. Proteins encoded by the human c-myc oncogene: differential expression in neoplastic cells. Mol Cell Biol 1984;4:2486–97.
29. Grandori C, Cowley SM, James LP, Eisenman RN. The Myc/Max/Mad network and the transcriptional control of cell behavior. Annu Rev Cell Dev Biol 2000;16:653–99.
30. Swarbrick A, Akerfeldt MC, Lee CS, Sergio CM, Caldon CE, Hunter LJ, et al. Regulation of cyclin expression and cell cycle progression in breast epithelial cells by the helix-loop-helix protein Id1. Oncogene 2005;24:381–9.
31. Geng H, Rademacher BL, Pittsenbarger J, Huang CY, Harvey CT, Lafortune MC, et al. Id1 enhances docetaxel cytotoxicity in prostate cancer cells through inhibition of p21. Cancer Res 2010;70: 3239–48.
32. Vita M, Henriksson M. The Myc oncoprotein as a therapeutic target for human cancer. Semin Cancer Biol 2006;16:318–30.
33. Zeller KI, Zhao XD, Lee CWH, Chiu KP, Yao F, Yustein JT, et al. Global mapping of c-Myc binding sites and target gene networks in human B cells. Proc Natl Acad Sci U S A 2006;103:17834–9.
34. Reichert M, Saur D, Hamacher R, Schmid RM, Schneider G. Phosphoinositide-3-kinase signaling controls S-phase kinase-associated protein 2 transcription via E2F1 in pancreatic ductal adenocarcinoma cells. Cancer Res 2007;67:4149–56.
35. Larrea MD, Wander SA, Slingerland JM. p27 as Jekyll and Hyde: regulation of cell cycle and cell motility. Cell Cycle 2009;8:3455–61.
36. Sandgren EP, Quaife CJ, Pinkert CA, Palmiter RD, Brinster RL. Oncogene-induced liver neoplasia in transgenic mice. Oncogene 1989;4: 715–24.
37. Murakami H, Sanderson ND, Nagy P, Marino PA, Merlino G, Thorgeirsson SS. Transgenic mouse model for synergistic effects of nuclear oncogenes and growth factors in tumorigenesis: interaction of c-myc and transforming growth factor alpha in hepatic oncogenesis. Cancer Res 1993;53:1719–23.
38. Saddic LA, Wirt S, Vogel H, Felsher DW, Sage J. Functional interactions between retinoblastoma and c-Myc in a mouse model of hepatocellular carcinoma. PLos ONE 2011;6:e19758.
39. Zimonjic DB, Popescu NC. Role of Dlc1 tumor suppressor gene and Myc oncogene in pathogenesis of human hepatocellular carcinoma: potential prospects for combined targeted therapeutics. Int J Oncol 2012;41:393–406.
40. Santoni-Rugiu E, Preisegger KH, Kiss A, Audolfsson T, Shiota G, Schmidt EV, et al. Thorgeirsson S.S. Inhibition of neoplastic development in the liver by hepatocyte growth factor in a transgenic mouse model. Proc Natl Acad Sci U S A 1996;93:9577–82.

The American Journal of Pathology, Vol. 183, No. 3, September 2013

ELSEVIER

The American Journal of
PATHOLOGY

ajp.amjpathol.org

CARDIOVASCULAR, PULMONARY, AND RENAL PATHOLOGY

Qualitative Rather than Quantitative Changes Are Hallmarks of Fibroblasts in Bleomycin-Induced Pulmonary Fibrosis

Tatsuya Tsukui,*† Satoshi Ueha,*† Jun Abe,*† Shin-ichi Hashimoto,*† Shigeyuki Shichino,*† Takeshi Shimaoka,*† Francis H.W. Shand,‡ Yasuka Arakawa,*† Kenshiro Oshima,§ Masahira Hattori,§ Yutaka Inagaki,†¶ Michio Tomura,‖ and Kouji Matsushima*†

From the Department of Molecular Preventive Medicine, Graduate School of Medicine, University of Tokyo, Tokyo, Japan; the Japan Science and Technology Agency—CREST Program,† Tokyo, Japan; the Department of Pharmacology,‡ University of Melbourne, Parkville, Australia; the Department of Computational Biology,§ Graduate School of Frontier Sciences, University of Tokyo, Chiba, Japan; the Research Unit for Tissue Remodeling and Regeneration,¶ Tokai University School of Medicine, Kanagawa, Japan; and the Center for Innovation in Immunoregulative Technology and Therapeutics,‖ Kyoto University Graduate School of Medicine, Kyoto, Japan*

Accepted for publication June 3, 2013.

Address correspondence to Kouji Matsushima, M.D., Ph.D., Department of Molecular Preventive Medicine, Graduate School of Medicine, The University of Tokyo, 7-3-1, Hongo, Bunkyo-ku, Tokyo 113-0033, Japan. E-mail: koujim@m.u-tokyo.ac.jp.

Pulmonary fibrosis is characterized by accumulation of activated fibroblasts that produce excessive amounts of extracellular matrix components such as collagen type I. However, the dynamics and activation signatures of fibroblasts during fibrogenesis remain poorly understood, especially *in vivo*. We examined changes in lung tissue cell populations and in the phenotype of activated fibroblasts after acute injury in a model of bleomycin-induced pulmonary fibrosis. Despite clustering of collagen type I-producing fibroblasts in fibrotic regions, flow cytometry-based quantitative analysis of whole lungs revealed that the number of fibroblasts in the lungs remained constant. At the peak of inflammation, fibroblast proliferation and apoptosis were both increased, suggesting that the clustering was not merely a result of proliferation, but also of fibroblast migration from nearby alveolar walls. Parabiosis experiments demonstrated that fibroblasts were not supplied from the circulation. Comprehensive gene expression analysis of freshly isolated fibroblasts revealed a detailed activation signature associated with fibrogenesis, including changes in genes responsible for migration and extracellular matrix construction. The *Spp1* gene, which encodes osteopontin, was highly up-regulated and was an identifying characteristic of activated fibroblasts present at the sites of remodeling. Osteopontin may serve as a useful marker of profibrotic fibroblasts. These results provide insights into the cellular and molecular mechanisms underlying pulmonary fibrosis and provide a foundation for development of specific antifibrotic therapies. *(Am J Pathol 2013, 183: 758–773; http://dx.doi.org/10.1016/j.ajpath.2013.06.005)*

Fibrosis is a common pathological feature of chronic inflammation. In response to injury, activated fibroblasts accumulate in damaged tissue and irreversibly deposit excessive amounts of extracellular matrix (ECM) components, which severely impair organ function.[1] In the lungs, the most common fibrotic disease is idiopathic pulmonary fibrosis, which is characterized by a histological pattern of usual interstitial pneumonia including bronchiolization and honeycombing. Because means for early diagnosis and effective therapies are lacking for idiopathic pulmonary fibrosis, patients have a median survival of only 2.5 to 3.5 years after diagnosis.[2]

Within fibrotic lesions, fibroblastic cells are activated by cytokines and growth factors such as TGF-β, often expressing α-smooth muscle actin (α-SMA) and adopting a myofibroblast phenotype. As the major producers of ECM components such as collagen type I, myofibroblasts play a central role in the pathogenesis of fibrosis.[3,4] Myofibroblasts derive from several types of progenitor cells, depending on the organ and experimental model. Although resident fibroblasts have been considered the major progenitors of myofibroblasts in the lungs, the extent of the contribution of other cell populations, such as epithelial cells or fibrocytes, remains a matter of debate.[5–8] Hoyles et al[9] found that resident fibroblast-specific deletion of the high-affinity type II TGF-β receptor attenuated bleomycin-induced lung fibrosis,

Supported by the Japan Science and Technology Agency (CREST Program).

http://dx.doi.org/10.1016/j.ajpath.2013.06.005

demonstrating the important role of resident fibroblasts in their model. Rock et al[10] recently used genetic lineage labeling to demonstrate that type II alveolar cells and Scgb1a1-positive cells (mainly bronchiolar Clara cells) in the alveoli and bronchioles did not become myofibroblasts through epithelial–to-mesenchymal transition in bleomycin-induced lung fibrosis. They also showed that NG2-expressing pericyte-like cells (which are sources of myofibroblasts in some fibrosis models[11,12]) were not major progenitors of myofibroblasts in the lungs. Nonetheless, there remains a need to clarify the role of resident fibroblasts as myofibroblast progenitors in the lungs.

Resident fibroblasts, which comprise 30% to 40% of tissue cells in the lungs, form scaffolds for alveoli by secreting ECM components.[13] Despite the prevalence of these cells in the alveoli and despite their postulated roles in pulmonary fibrosis, the *in vivo* properties of resident fibroblasts in both their normal and activated states remain poorly understood. Fibroblasts lack specific surface markers, and stromal cell heterogeneity in lung has not been well characterized. Earlier studies have often isolated fibroblasts by their adhesiveness to plastic dishes, which in itself can affect the phenotype of fibroblasts.[14] In addition, the histological approaches that are commonly used in fibrosis studies have limited parameters and resolution for the quantitative analysis of single cells. For these reasons, it remains largely unknown how fibroblasts generate fibrotic lesions and contribute to organ fibrosis. To develop novel therapies for pulmonary fibrosis that specifically suppress fibroblast activation, accumulation, and ECM deposition, a more detailed picture of how these processes occur is required.

In the present study, we analyzed qualitative and quantitative changes in fibroblast populations in a model of bleomycin-induced lung fibrosis. Fibroblasts were identified using collagen type I, alpha 2 (*Col1a2*) reporter mice, in which collagen type I-expressing fibroblasts are labeled with EGFP.[15,16] Flow-cytometric analysis of cells from enzymatically dissociated lung tissue taken during bleomycin-induced lung fibrosis revealed phenotypic changes without a change in overall fibroblast numbers. Although fibroblast proliferation increased, this was countered by a similar increase in apoptosis. On the other hand, gene expression profiles of freshly isolated fibroblasts generated by next-generation DNA sequencing revealed a detailed gene signature for profibrotic cells. Specifically, the gene encoding osteopontin (OPN) was highly up-regulated, suggesting that OPN may serve as an activation marker of lung fibroblasts.

Materials and Methods

Mice

Col1a2-GFP (C57BL/6 background for ≥10 generations) and ROSA-CAG-SCAT3.1 mice were generated in previous studies.[16,17] ROSA-CAG-SCAT3.1 mice were generated with BDF1-derived ES cells and backcrossed to C57BL/6 mice for at least two generations.[17] The properties of FucciG1-#639 and FucciS/G2/M-#474 mice (both C57BL/6 background) are to be published elsewhere. C57BL6/J mice were purchased from Japan SLC (Hamamatsu, Japan) or CLEA Japan (Tokyo, Japan). Animal experiments were performed on 6- to 12-week–old mice. Mice were bred and maintained in specific pathogen-free facilities at the University of Tokyo. All animal experiments were performed in accordance with the guidelines of the Animal Care and Use Committee of the University of Tokyo.

Intratracheal Instillation

Mice were anesthetized with pentobarbital. Bleomycin sulfate (1.25 to 2.5 mg/kg dissolved in 50 μL of saline solution; Toronto Research Chemical, Toronto, ON, Canada) or 50 μg lipopolysaccharide from *Salmonella minnesota* R595 (Enzo Life Sciences, Farmingdale, NY) were instilled intratracheally by oropharyngeal aspiration.[18]

BrdU

Bromodeoxyuridine (BrdU; 0.8 mg in 200 μL saline; Sigma-Aldrich, Tokyo, Japan; St. Louis, MO) was injected intraperitoneally at 24 hours before sacrifice. Mouse drinking water was supplemented with 0.8 mg/mL BrdU for this 24-hour period. For long-term BrdU pulse experiments, mice were injected with 0.8 mg BrdU i.p. after bleomycin treatment and given 0.8 mg/mL BrdU-containing drinking water until analysis.

Tissue Dissociation

Mice were anesthetized with pentobarbital. After perfusion with 5 mL of PBS via the right ventricle, the trachea was cannulated. Pulmonary airspaces were lavaged three times with 1 mL PBS each time. Either the left or right lobes of the lungs were harvested for flow cytometry. The lobes were cut into small pieces and digested in protease solution [0.2% collagenase (Wako Pure Chemical Industries, Osaka, Japan), 0.1 mg/mL Dispase II (Roche, Basel, Switzerland), and 2000 U/mL DNase I (Merck, Darmstadt, Germany) in RPMI medium (Sigma-Aldrich)] for 60 minutes at 37°C with trituration by micropipette every 20 minutes. After being passed through a 70-μm strainer (BD Biosciences, San Diego, CA), cells were washed and resuspended in RPMI medium (Sigma-Aldrich) containing 10% fetal bovine serum. Peripheral blood cells were treated with red blood cell lysis buffer before analysis by flow cytometry.

Hydroxyproline Assay

Lung hydroxyproline content was measured as described previously.[19,20] In brief, mice were sacrificed and the left lungs were harvested. The lungs were minced and suspended in up to 800 μL of ultrapure water, after which 800 μL of

12 N HCl was added and the mixture heated for 24 hours at 110°C. The resulting acid hydrolysates was filtrated through a 0.45-μm filter, and 25 μL was transferred to new tubes. Next, 25 μL of 6 N NaOH, 50 μL of citric acetate buffer (5% citric acid, 7.24% sodium acetate, 3.4% NaOH, 1.2% glacial acetic acid, pH 6.0), and 400 μL of chloramine T solution (564 mg of chloramine T, 4 mL of H_2O, 4 mL of *n*-propanol, and 32 mL of citric-acetate buffer) were added, and the mixture was incubated for 20 minutes at room temperature. Next, 400 μL of Ehrlich's solution (4.5 g of 4-dimethylaminobenzaldehyde, 18.6 mL of *n*-propanol, and 7.8 mL of 70% perchloric acid) was added, and the mixture was incubated for a further 15 minutes at 65°C before the absorbance (optical density OD_{550}) of the solution was measured. The reagents were purchased from Wako Pure Chemical Industries, Sigma-Aldrich Japan, and Tokyo Chemical Industry (Tokyo, Japan).

Flow Cytometry

Cell suspensions were incubated with anti-CD16/32 antibody to block nonspecific binding, followed by PerCP-Cy5.5 anti-CD31, phycoerythrin (PE)-Cy7 anti-EpCAM, and allophycocyanin (APC)-Cy7 anti-Ter119 antibodies from Biolegend (San Diego, CA) and APC anti-CD45.2 antibody from BD Biosciences (San Jose, CA). For α-SMA and cleaved caspase 3 intracellular staining, cells were fixed with Cytofix/Cytoperm buffer (BD Biosciences) for 20 minutes before incubation with APC anti-α-SMA antibody (R&D Systems, Minneapolis, MN) and anti-cleaved caspase 3 (Cell Signaling Technology, Danvers, MA), followed by incubation with Alexa Fluor 647 anti-rabbit IgG (Life Technologies, Tokyo, Japan; Carlsbad, CA) for cleaved caspase 3. BrdU incorporation was examined using a BrdU flow kit (BD Biosciences). For intracellular OPN staining, single-cell suspensions were cultured in 10% fetal bovine serum–RPMI medium (Sigma-Aldrich) at 37°C with or without the protein transport inhibitor brefeldin A (BFA) for 6 hours, after which adherent cells were collected using trypsin–EDTA. After a washing, the cells were fixed with Cytofix/Cytoperm buffer (BD Biosciences) and then stained with goat anti-OPN primary antibodies (R&D Systems), followed by Alexa Fluor 647 anti-goat IgG as secondary antibody (Life Technologies). Antibody-labeled cells were washed twice before analysis with a Gallios flow cytometer (Beckman Coulter, Brea, CA). For analysis of cells from SCAT3.1 mice, the FL10 filter was switched to 525BP. Cell sorting was performed on FACSAria (BD Biosciences). Flow cytometry data were analyzed using FlowJo version 7.6.5 software (Tree Star, Ashland, OR).

Immunohistochemistry

Lungs were fixed with 4% paraformaldehyde–PBS for 6 hours at 4°C, treated with 30% sucrose for cryoprotection, and then embedded in TissueTek optimal cutting temperature compound (Sakura Finetek Japan, Tokyo, Japan). For OPN staining, lungs were filled through the trachea with BFA containing 10% fetal bovine serum-RPMI medium (Sigma-Aldrich) and were incubated in the same medium at 37°C for 6 hours, before paraformaldehyde fixation. Frozen sections (6 μm thick) were stained with PE anti-EpCAM (Bio-Legend), APC anti–α-SMA (R&D Systems), anti-collagen type I (Cosmo Bio, Tokyo, Japan), anti-CD45 (BD Biosciences), and anti-OPN (R&D Systems) primary antibodies, followed by incubation with Alexa Fluor 647 anti-rabbit IgG for collagen type I, Alexa Fluor 546 anti-rat IgG for CD45, and Alexa Fluor 647 anti-goat IgG for OPN (Life Technologies). For BrdU staining, sections were incubated in 500 U/mL DNase (Calbiochem; EMD Millipore, Billerica, MA) solution for 60 minutes at 37°C to retrieve the antigen before staining. Sections were mounted with ProLong Gold antifade reagent (Life Technologies), in some cases containing 2 μg/mL propidium iodide (PI). Sections were photographed using an SP5 confocal microscope (Leica Microsystems, Wetzlar, Germany).

SAGE

Gene expression analysis was performed using serial analysis of gene expression (SAGE) and next-generation sequencing with an Ion Torrent Personal Genome Machine (PGM) sequencer (Life Technologies). Lung tissue single-cell suspensions from three mice were pooled for each group, and lineage-negative (Lin^-) GFP^+ fibroblasts were isolated by cell sorting. RNA was isolated from these cells using a *mir*Vana miRNA isolation kit (Life Technologies). The next-generation sequencing data were generated from 1 μg of total RNA. SAGE libraries were constructed using a SOLiD SAGE kit (Life Technologies) according to the manufacturer's protocol. DNA was recovered from the agarose gel using a PureLink gel extraction kit (Life Technologies). DNA fragments of SAGE construct were analyzed on an Agilent 2100 Bioanalyzer platform using a high-sensitivity kit (Agilent Technologies, Santa Clara, CA). Template preparation, emulsion PCR, and Ion Sphere particle enrichment was performed using an Ion Xpress Template kit (Life Technologies) according to the manufacturer's instructions. The quality of the resultant Ion Sphere particle was assessed using a Qubit 2.0 fluorometer (Life Technologies) before the particles were loaded onto a 318 chip (Life Technologies) for sequencing. Raw data from these experiments have been deposited in the NCBI Gene Expression Omnibus (*http://www.ncbi.nlm.nih.gov/geo*; accession number GSE42564).

Mapping of Next-Generation Sequencing Data

For each sample, raw reads from the PGM sequencer were aligned against mouse RefSeq genes (*http://hgdownload.cse.ucsc.edu/goldenpath/mm9/database*) using Burrows-Wheeler alignment software, version 0.6.2, which uses the 25_1 mapping parameter. We generated unique gene counts

by excluding reads that mapped to contigs of more than one gene; reads mapping to several contigs within an isogroup were counted only once. To include only highly expressed genes and to avoid high dispersion, genes with fewer than 50 tags in both saline-treated and bleomycin-treated groups were eliminated from the library before analysis. Gene ontology (GO) analysis was performed using DAVID (Database for Annotation, Visualization and Integrated Discovery) Bioinformatic Resources software version 6.7 (*http://david.abcc.ncifcrf.gov/home.jsp*).[21] Pathway analysis was performed using IPA software version 9.0 (Ingenuity Systems, Redwood City, CA).

qPCR Analysis

A portion of the mRNA isolated for SAGE was reverse-transcribed to cDNA using a Life Technologies high-capacity reverse transcription kit. Quantitative real-time PCR (qPCR) analysis was performed using SYBR Green detection of amplified products and an ABI 7500 real-time PCR system (Life Technologies). Primers used for qPCR were as follows: GAPDH forward 5′-AGTATGACTCCACTCACGGCAA-3′ and reverse 5′-TCTCGCTCCTGGAAGATGGT-3′; Spp1 forward 5′-GGAGGAAACCAGCCAAGG-3′ and reverse 5′-TGCCAGAATCAGTCACTTTCAC-3′; α-SMA forward 5′-CTGGAGAAGAGCTACGAACTGC-3′ and reverse 5′-CTGATCCACATCTGCTGGAAGG-3′; S100a4 forward 5′-GGAGCTGCCTAGCTTCCTG-3′ and reverse 5′-TCCTGGAAGTCAACTTCATTGTC-3′; Tnc forward 5′-GGGCTATAGAACACCGATGC-3′ and reverse 5′-CATTTAAGTTTCCAATTTCAGGTTC-3′; Fn1 forward 5′-CGGAGAGAGTGCCCCTACTA-3′ and reverse 5′-CGATATTGGTGAATCGCAGA-3′; Ereg forward 5′-TTGACGCTGCTTTGTCTAGG-3′ and reverse 5′-GGATCACGGTTGTGCTGAT-3′; Sfrp1 forward 5′-CAGTTGTGGCTTTTGCATTG-3′ and reverse 5′-GAGGGAAGGGAGAGGGTTC-3′; Pcolce2 forward 5′-CAAATTCAGGCCGAAAAAGT-3′ and reverse 5′-CCACAGTGGGCTTTAGACCT-3′; Gsn forward 5′-CAAAGTCGGGTGTCTGAGG-3′ and reverse 5′-CTTCCCTGCCTTCAGGAAT-3′; and Efemp1 forward 5′-CCACAGGGTTACGAAGTGGT-3′ and reverse 5′-TCATTGGTGGTCTCACATTCA-3′.

Statistical Analysis

Statistical comparisons were performed using unpaired *t*-tests (two-tailed). A P value of <0.05 was considered statistically significant. Data are expressed as means ± SEM.

Results

Characterization of GFP$^+$ Cells in the Lungs of Col1a2-GFP Mice

We first investigated what kinds of cells were labeled with GFP in lungs of Col1a2-GFP reporter mice.[16] Lungs were dissociated with a protease solution and analyzed by multicolor flow cytometry. GFP$^+$ cells comprised a distinct population that was negative for the lineage markers Ter119 (data not shown), CD45, CD31, and EpCAM (Figure 1A). Approximately 70% to 80% of Lin$^-$ GFP$^+$ cells were PDGFRα$^+$; the remainder were PDGFRα$^-$ (Figure 1B). Immunofluorescence imaging of lung sections revealed GFP$^+$ cells to be present in alveolar walls and in peribronchiolar and perivascular regions (Figure 1C). The peribronchiolar and perivascular GFP$^+$ cells also expressed α-SMA, consistent with these being smooth muscle cells (Figure 1C).[15] Alveolar GFP$^+$ cells were located in the interstitium, surrounded by basement membranes manifested by collagen type IV (Figure 1D). Previous studies have demonstrated that alveolar fibroblasts are PDGFRα$^+$, NG2$^-$, α-SMA$^-$, and CD31$^-$,[10,22] a phenotype consistent with that observed in alveolar GFP$^+$ cells. In summary, GFP$^+$ cells in Col1a2-GFP mice comprise a mixed population of alveolar fibroblasts and smooth muscle cells, with alveolar fibroblasts constituting the majority.

Quantitative Analysis of Lung Tissue Cell Dynamics

A prominent characteristic of pulmonary fibrosis is the accumulation of activated fibroblasts/myofibroblasts in fibrotic lesions. This is caused by the migration of fibroblasts into alveolar spaces and their subsequent proliferation.[23] Previous studies have demonstrated BrdU uptake of interstitial cells in fibrotic lesions and enhanced *in vitro* proliferative capacity of fibroblasts from fibrotic organs.[24–26] However, it remains to be shown *in vivo* whether this increase in fibroblast numbers mediates the excessive deposition of ECM during fibrosis.

We used a bleomycin-induced lung fibrosis model in Col1a2-GFP mice to investigate changes that occur in lung tissue cell populations. The extent of lung fibrosis occurring in this model was verified by the measurement of hydroxyproline and the expression of profibrotic genes in whole lungs (Supplemental Figure S1). Numbers of leukocytes and of tissue cells such as endothelial cells, epithelial cells, and fibroblasts were determined by multicolor flow cytometry (Figure 2A). The number of CD45$^+$ leukocytes in the lungs was elevated at days 7 and 14 after bleomycin administration (Figure 2B), which may reflect the infiltration of inflammatory cells. CD31$^+$ endothelial cell numbers did not change significantly after bleomycin administration (Figure 2B). In contrast, EpCAM$^+$ epithelial cells, a population that includes alveolar type II cells, bronchiolar epithelial cells, and possibly alveolar type I cells,[27] markedly decreased after bleomycin treatment (Figure 2B). This probably resulted from the denudation of the epithelium that is induced by bleomycin toxicity. Contrary to expectations, the numbers of Lin$^-$ GFP$^+$ fibroblasts in whole-lung tissue preparations remained constant throughout bleomycin-induced lung fibrosis (Figure 2B). Even at days 14 and 21 after bleomycin administration, which fall within the peak

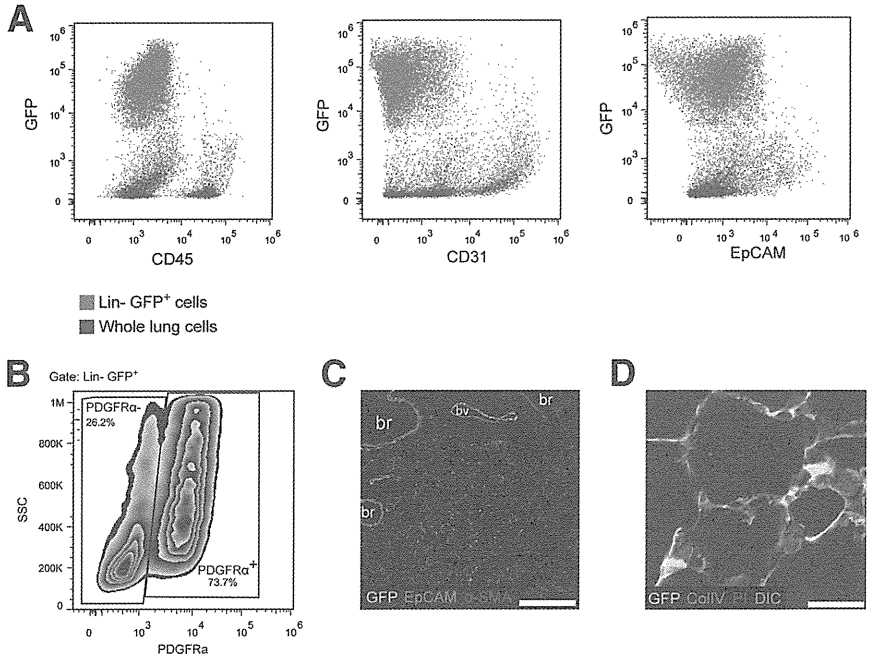

Figure 1 Characterization of GFP$^+$ cells in the lungs of Col1a2-GFP mice. **A:** Lung single-cell suspensions were stained with antibodies against CD45, CD31, and EpCAM. Lin$^-$ (ie, Ter119$^-$ CD45$^-$ CD31$^-$ EpCAM$^-$) GFP$^+$ cells (red) made up a distinctive CD45$^-$ CD31$^-$ EpCAM$^-$ population. **B:** Lin$^-$ GFP$^+$ cells comprised 70% to 80% PDGFRα^+ cells and 20% to 30% PDGFRα^- cells. **C:** Lung sections from Col1a2-GFP mice stained for EpCAM (red) and α-SMA (blue). **D:** Lung sections from Col1a2-GFP mice stained for collagen type IV (red) and PI (blue). Differential interference contrast (DIC) is also shown (gray). Scale bars: 400 μm (**C**); 25 μm (**D**). br, bronchiole; bv, blood vessel.

period for fibrosis,[28] there was no difference in Lin$^-$ GFP$^+$ fibroblast numbers, compared with saline-treated control (Figure 2C), nor was any increase in fibroblast number observed at day 28 (data not shown).

To technically validate these results, we used the lipopolysaccharide-induced acute lung injury model as a negative control in which an increase in fibroblasts is not expected. We observed a massive increase in leukocyte infiltration into the lungs and alveolar air spaces after lipopolysaccharide administration, but the numbers of lung tissue cells including fibroblasts remained unchanged (Supplemental Figure S2). In the absence of a suitable positive control model in which an increase in lung fibroblasts would be expected, we used a tumor lung metastasis model to confirm that increases in lung tissue cells could be detected. At 18 days after intravenous injection of 4×10^6 Lewis lung carcinoma cells (3LL cells), we observed a dramatic increase in EpCAM$^+$ tumor cells without any increase in the other tissue cell populations (Supplemental Figure S3). These results indicate that flow-cytometric analysis after complete digestion of lung tissue is an appropriate way to quantify tissue cell numbers. Thus, the excessive accumulation of ECM that occurs during lung fibrosis cannot be accounted for by an increase in fibroblast numbers.

Qualitative Changes in Fibroblasts after Bleomycin Treatment

Previous studies have shown that exposure of fibroblasts to bleomycin induces an activated phenotype that includes increased α-SMA and collagen type I expression.[4] However, these studies identified fibroblasts only by their stromal localization or by their adhering plastic dishes. Because there was no quantitative increase in fibroblast numbers during fibrosis, we next examined whether there are any phenotypic changes in collagen type I–producing fibroblasts after bleomycin treatment. At day 14, we observed a greater proportion of GFP^{hi} fibroblasts in bleomycin-treated mice, which indicates increased expression of Col1a2 (Figure 3A). GFP^{hi} fibroblasts had high side scatter (SSC) (Figure 3A). Furthermore, many SSC^{hi} fibroblasts had increased forward scatter (FSC) (Figure 3B). Of the bleomycin-treated fibroblasts in the GFP^{hi} SSC^{hi} gate (Figure 3A), 77.3 ± 2.5% also fell into the FSC^{hi} SSC^{hi} gate (Figure 3B), compared with 44.2 ± 2.3% of saline-treated fibroblasts (data not shown) ($P < 0.01$). These data suggest that cell size and intracellular organelle complexity increase in activated fibroblasts. These changes were also quantifiable as greater mean fluorescent intensity values for GFP, SSC, and FSC in Lin$^-$ GFP$^+$ cells from bleomycin-treated mice (Figure 3C).

To investigate whether Lin$^-$ GFP$^+$ fibroblasts differentiate into myofibroblasts, we also measured α-SMA expression by flow cytometry (Figure 3D). In normal lungs (day 0), 4.41 ± 0.49% of Lin$^-$ GFP$^+$ cells were α-SMA$^+$ (Figure 3D), probably representing peribronchiolar and perivascular smooth muscle cells (Figure 3E). At days 7 and 14 after bleomycin administration, the proportion of α-SMA$^+$ cells was almost twice as high as at day 0 (Figure 3D). By day 21, however, the proportion of α-SMA$^+$ cells had returned to normal levels, which is consistent with previous studies.[10,29]

Histological Analysis of Col1a2-GFP Mouse Lungs

Flow-cytometric analysis of fibroblasts revealed clear phenotypic changes associated with activation by bleomycin. We next investigated whether these changes could be observed histologically. In saline-treated lungs, α-SMA expression was confined to peribronchiolar and perivascular

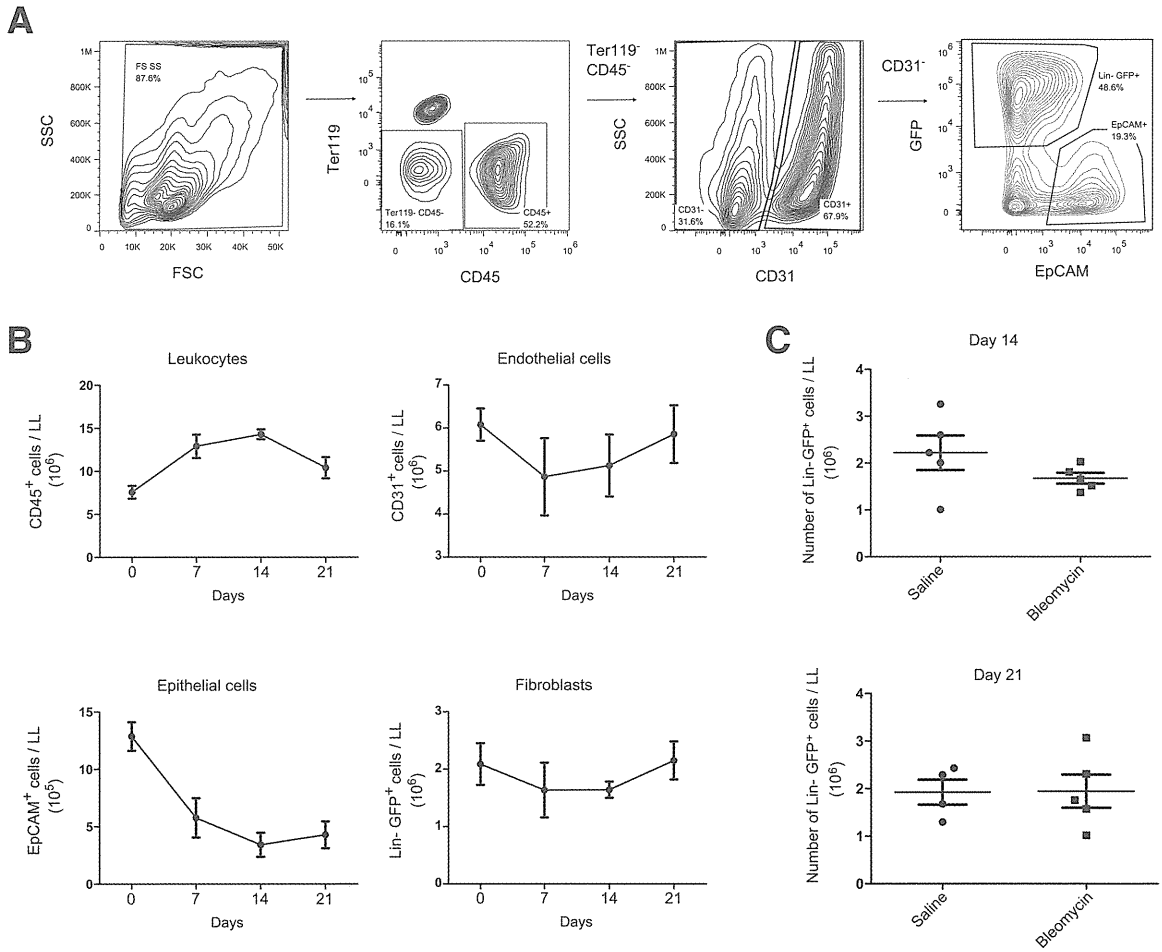

Figure 2 Changes in lung tissue cell populations during bleomycin-induced pulmonary fibrosis. **A:** Enzymatically dissociated lung cells from bleomycin-treated Col1a2-GFP mice were stained for lineage markers and analyzed by flow cytometry. **B:** $CD45^+$ leukocytes, $CD31^+$ endothelial cells, $EpCAM^+$ epithelial cells, and Lin^- GFP^+ fibroblasts were quantified by flow cytometry at 7, 14, and 21 days after bleomycin administration. Day 0 data were from untreated mice. **C:** Numbers of Lin^- GFP^+ cells in the lungs did not differ between saline- or bleomycin-treated mice at 14 and at 21 days after bleomycin administration, as quantified by flow cytometry. Data are expressed as means ± SEM (**B**) or as both means ± SEM and individual data points (**C**). n = 3 or 4 (**B**); 4 or 5 (**C**). LL, left lobe.

smooth muscle cells, with most alveolar fibroblasts negative for α-SMA (Figure 3E). At day 14 after bleomycin treatment, there were a large number of GFP^+ fibroblast clusters (Figure 3E), in which the fibroblasts were surrounded by extracellular collagen type I (Figure 3F). Thus, bleomycin treatment induced the formation of fibrotic regions made up of fibroblast clusters. Many of the GFP^+ fibroblasts in these clusters were α-SMA^+ (Figure 3E), suggesting that these cells were actually myofibroblasts. In bleomycin-treated lungs, α-SMA expression extended beyond the peribronchiolar and perivascular regions into the alveolar region, in accord with the greater numbers of GFP^+ α-SMA^+ cells detected by flow cytometry. The fibroblasts making up the fibrotic regions observed at day 14 after bleomycin treatment had relatively large cell sizes, compared with those in saline-treated lungs (Figure 3E). Taken together with the increase of GFP^+ α-SMA^+ cells detected by flow cytometry (Figure 3D), these results suggest a tendency for GFP^+ alveolar fibroblasts to differentiate into myofibroblasts after bleomycin treatment. These results also suggest that GFP^+ fibroblasts play a central role in the formation of fibrotic regions.

Proliferation and Apoptosis of Fibroblasts after Bleomycin Treatment

Despite lack of change in absolute numbers of lung fibroblasts after treatment with bleomycin, as measured by flow cytometry, GFP^+ fibroblasts in bleomycin-treated lungs displayed clustering and increased cell density in fibrotic regions, which is suggestive of a proliferative response. These conflicting results led us to hypothesize that both proliferation and cell death were accelerated during fibrosis in the lungs, in balance with each other. To examine fibroblast apoptosis, we investigated the activation of caspase 3 using an anti-cleaved caspase 3 antibody (Figure 4A). We treated Col1a2-GFP mice with bleomycin, then measured apoptosis of lung tissue cells by flow cytometry (Figure 4B). Only a very small proportion (0.1% to 0.8%) of endothelial cells were apoptotic during bleomycin-induced fibrosis

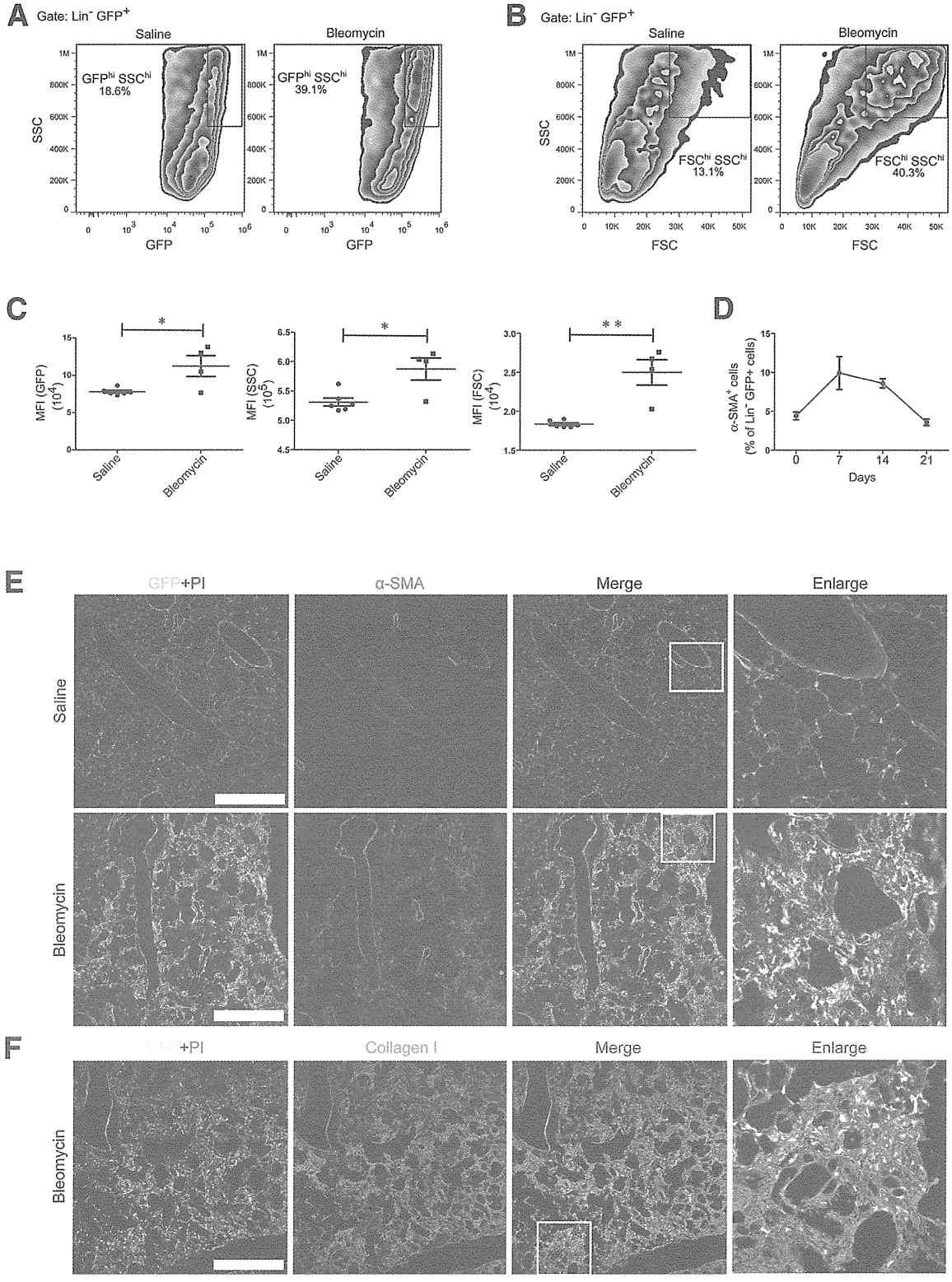

Figure 3 Qualitative changes in fibroblasts during bleomycin-induced lung fibrosis. **A** and **B**: Lung cells from Col1a2-GFP mice at 14 days after saline or bleomycin administration were stained for lineage markers. Lin^- GFP^+ fibroblasts were plotted as SSC versus GFP (**A**) and SSC versus FSC (**B**). **C**: The mean fluorescent intensities (MFI) of GFP, SSC, and FSC signals of Lin^- GFP^+ fibroblasts from Col1a2-GFP mice at 14 days after saline or bleomycin administration. **D**: Lung cells from Col1a2-GFP mice at 0, 7, 14, and 21 days after bleomycin administration were stained for lineage markers and α-SMA and the proportion of α-SMA^+ cells was evaluated by flow cytometry. **E** and **F**: Lungs from Col1a2-GFP mice at 14 days after saline (**E**) or bleomycin (**E** and **F**) administration were stained with antibodies against PI and α-SMA (**E**) or PI and collagen type I (**F**). **Boxed** regions in the Merge column correspond to images in the Enlarge column. Original magnification, ×400. Data are expressed as means ± SEM (**D**) or as both means ± SEM and individual data points (**C**). $n = 4$ or 6 (**C**); $n = 3$ or 4 (**D**). $^*P < 0.05$, $^{**}P < 0.01$. Scale bar = 500 μm.

(Figure 4B). In contrast, the proportion of epithelial cells that were apoptotic dramatically increased after bleomycin treatment, from 1.3 ± 0.2% in untreated mice to 6.0 ± 0.3% on day 14 after bleomycin treatment (Figure 4B). This result highlights the severe injury sustained by the lung epithelium during bleomycin-induced fibrosis. Unlike endothelial and epithelial cells, in GFP$^+$ fibroblasts the apoptosis peaked at day 7, although the proportion of apoptotic cells observed on day 14 remained elevated above those seen at day 0 (Figure 4B).

We also examined the apoptosis of tissue cells using ROSA-CAG-SCAT3.1 knockin mice (SCAT3.1 mice), in which apoptotic cells are detected with fluorescent fusion protein.[17,30,31] In these mice, apoptotic cells form a population with a reduced fluorescence resonance energy transfer (FRET) signal and a slightly elevated ECFP signal, compared with nonapoptotic cells (Supplemental Figure S4). The kinetics of apoptosis obtained with SCAT3.1 mice were similar to those obtained with anti-cleaved caspase 3 antibody (Supplemental Figure S5). These results demonstrate the different sensitivities of tissue cells to apoptosis during the lung remodeling caused by bleomycin.

We next used BrdU to investigate the proliferation of lung tissue cells during bleomycin-induced fibrosis. At 24 hours after bleomycin-treated Col1a2-GFP mice were injected intraperitoneally with BrdU, their lungs were harvested and the number of BrdU$^+$ cells present was counted by flow cytometry (Figure 4C). Uptake of BrdU by endothelial cells peaked at day 7 and then gradually decreased (Figure 4D). Uptake by epithelial cells similarly peaked at day 7, but was sustained at similar levels at days 14 and 21 (Figure 4D). GFP$^+$ fibroblasts also had the greatest BrdU incorporation at 7 days after bleomycin administration, followed by a steady decrease across days 14 and 21 (Figure 4D), a pattern similar

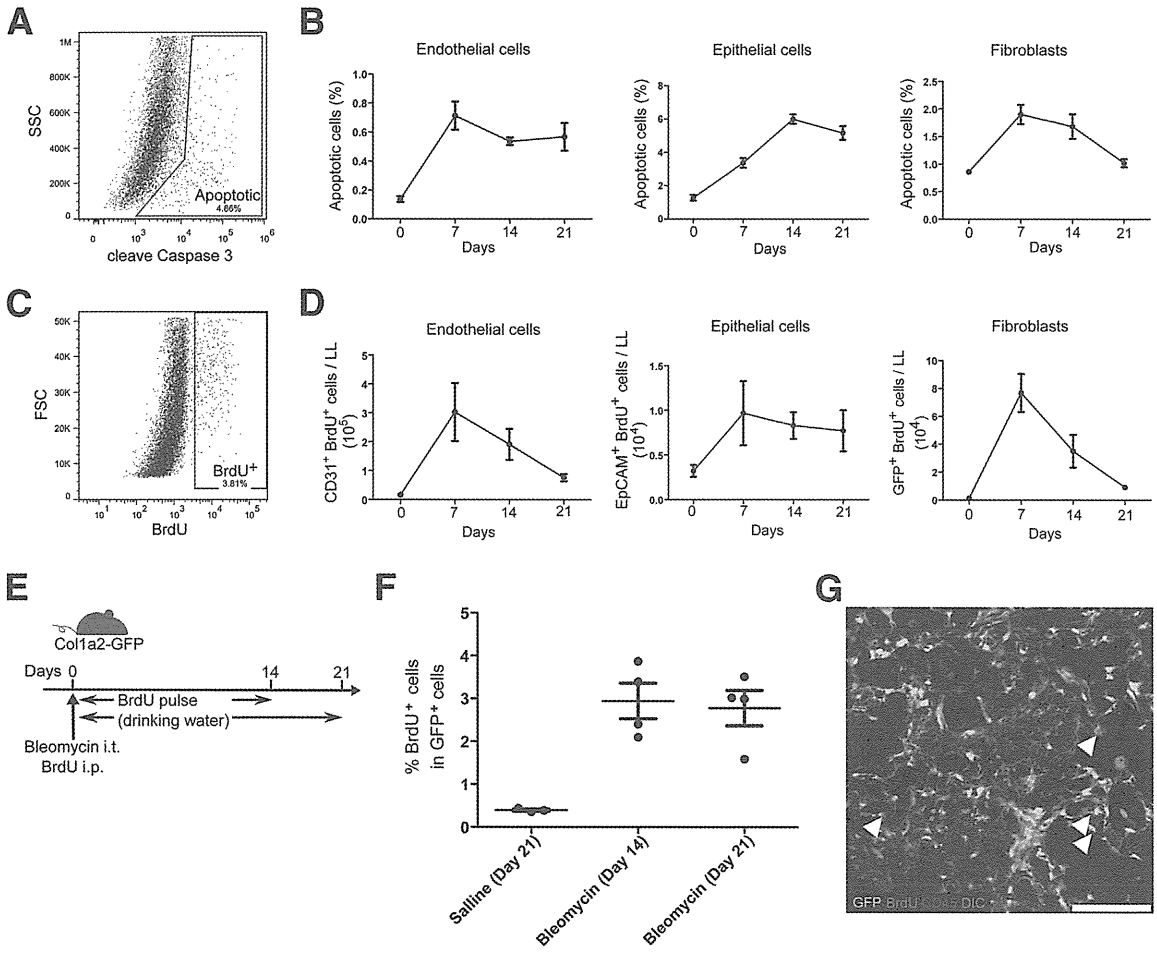

Figure 4 Proliferation and apoptosis of fibroblasts in bleomycin-induced pulmonary fibrosis. **A:** Identification of apoptotic cells by flow cytometry with anti-cleaved caspase 3 antibody. **B:** The proportion of apoptotic cells in different lung cell populations from Col1a2-GFP mice at 0, 7, 14, and 21 days after bleomycin administration was analyzed by flow cytometry after staining for CD31 (endothelial cells), EpCAM (epithelial cells), and CD45 (leukocytes). **C:** Identification of BrdU$^+$ cells by flow cytometry. **D:** Col1a2-GFP mice were pulsed with BrdU for 24 hours before analysis at 0, 7, 14, or 21 days after bleomycin administration. Lung cells were stained for BrdU and CD31, EpCAM, and CD45 and BrdU$^+$ cell numbers were quantitated. **E:** Experimental design for long-term BrdU pulse experiments. **F:** After long-term BrdU pulse, lung cells were stained for BrdU and analyzed for the proportion of BrdU$^+$ cells among GFP$^+$ cells. **G:** Representative lung section from Col1a2-GFP mice at 14 days after bleomycin administration and long-term BrdU pulse, with staining for GFP (green), BrdU (red), and CD45 (blue). BrdU$^+$ GFP$^+$ cells are indicated by **arrowheads**. DIC is also shown (gray). Data are expressed as means ± SEM (**B** and **F**) or as both means ± SEM and individual data points (**D**). n = 3 or 4. Scale bar = 100 μm.

to that observed for apoptotic Lin^- cells (Figure 4B). Similar experiments using fluorescent ubiquitination-based cell cycle indicator (Fucci) mice (FucciG1-#639 and FucciS/G2/M-#474 double-transgenic mice), which enable quantification of proliferating cells independent of pulse time,[32] yielded results consistent with those obtained from BrdU-uptake experiments (Supplemental Figure S6).

To examine whether GFP^+ fibroblast clusters are dependent on cell proliferation, we treated Col1a2-GFP mice with a long-term BrdU pulse after bleomycin treatment (Figure 4E). In this experiment, approximately 30% of $CD45^+$ leukocytes in the lungs were $BrdU^+$ at day 14 or 21 after bleomycin treatment (Supplemental Figure S7). More than 10% of endothelial and epithelial cells were $BrdU^+$ at day 21 after bleomycin treatment (Supplemental Figure S7). In contrast, only 3% of GFP^+ cells in bleomycin-treated mice (day 14 and 21) were $BrdU^+$ (Figure 4F). Immunofluorescence staining of lung sections from bleomycin-treated mice (day 14) revealed BrdU staining among $CD45^+$ leukocytes and other stromal cells, which might have included endothelial and epithelial cells (Figure 4G and Supplemental Figure S7). However, only a small portion of GFP^+ cells were $BrdU^+$ (Figure 4G), and most of the GFP^+ cells in fibrotic clusters were $BrdU^-$, suggesting that the clusters do not form through proliferation alone.

In summary, bleomycin treatment induced both apoptosis and proliferation of lung tissue cells. Although proliferative GFP^+ fibroblasts were detected, particularly in the early phase of fibrosis, the concurrent induction of apoptosis kept the overall number of GFP^+ fibroblasts constant, and for the most part the GFP^+ fibroblast clusters were not formed only by proliferation.

The Contribution of Bone Marrow-Derived Cells to the Lung GFP^+ Fibroblast Population

Several studies have reported that $CD45^+$ collagen type I-positive circulating mesenchymal cells (so-called fibrocytes) contribute to fibrogenesis after bleomycin-induced lung injury.[33,34] However, we detected almost no GFP^+ cells in the peripheral blood cells, most of which were $CD45^+$, of saline- or bleomycin-treated Col1a2-GFP mice at day 14 after treatment (Figure 5A). To investigate the extent to which lung GFP^+ fibroblasts were supplied from the bone marrow via the circulation, we generated parabiotic pairs composed of Col1a2-GFP ($CD45.2^+$) and congenic wild-type (WT; $CD45.1^+$) mice (Figure 5B). At 6 weeks after surgery, we treated mice with bleomycin or saline. Lungs were then harvested at day 21 after bleomycin treatment for analysis by flow cytometry. Chimerism of 40% to 60% (B-cell congenic markers) was observed, demonstrating that circulating blood was shared in the parabiotic mice (Figure 5C). However, in WT lungs only a very small proportion (<0.5%) of Lin^- cells were GFP^+ after treatment with either saline or bleomycin (Figure 5D). Similarly, fluorescent microscopy analysis of lung sections at 21 days after bleomycin treatment did not detect any GFP^+ fibroblasts in WT lungs, in stark contrast to the GFP^+ fibroblasts that were prominent in fibrotic regions of Col1a2-GFP lungs (Figure 5E). These results suggest that the GFP^+ fibroblasts in fibrotic regions in the lungs are not supplied from the bone marrow or the circulation during fibrosis. Instead, resident cells in the lungs, probably resident fibroblasts, are the likely progenitors of the activated fibroblasts that form fibrotic regions.

Gene Expression Analysis of GFP^+ Fibroblasts

To further investigate phenotypic changes in GFP^+ fibroblasts, we generated a whole-genome gene expression profile for these cells. We used next-generation sequencing to perform SAGE analysis on GFP^+ lung fibroblasts sorted by fluorescence-activated cell sorting at 14 days after saline or bleomycin treatment. The purity of GFP^+ cells after sorting was 94.5% and 98.0% for saline and bleomycin treatment, respectively. We identified 2,973,937 SAGE tags (1,080,798 tags from saline-treated GFP^+ fibroblasts and 1,893,139 tags from bleomycin-treated GFP^+ fibroblasts), representing 13,894 distinct transcripts. The number of tag sequences from bleomycin-treated GFP^+ fibroblasts was normalized to that of saline-treated GFP^+ fibroblasts before gene expression was compared between the two libraries. There were 213 genes with a greater than threefold difference between the saline and bleomycin groups. The 40 transcripts that increased the most after bleomycin treatment, compared with control, are listed in Table 1. The 40 genes that were most down-regulated are listed in Supplemental Table S1. The most highly up-regulated transcript (213-fold) was secreted phosphoprotein 1 (*Spp1*). To confirm the SAGE results, qPCR was performed for representative transcripts. There was good correlation between the results of the SAGE and qPCR analyses (Supplemental Figure S8).

Some of the 40 most up-regulated genes that were induced by bleomycin treatment have already been identified as important in fibrosis. *Spp1* is known to be up-regulated in idiopathic pulmonary fibrosis patients, as well as in the bleomycin-induced lung fibrosis model in mice.[35,36] Cytokine receptor-like factor 1 (*Crlf1*) expressed by epithelial cells was recently reported to have antifibrotic actions.[37] The present data, however, suggest that fibroblasts also express *Crlf1*. The expression of S100a4, a fibroblast marker, was low in saline-treated mice but dramatically up-regulated in bleomycin-treated mice. Gelsolin (*Gsn*), which is involved in the rearrangement of cytoskeletal structure and is necessary for the development of pulmonary fibrosis,[38] showed a remarkable decrease of tag number, from 19,346 to 2548 (Supplemental Table S1). Interestingly, expression of the latent transforming growth factor β binding protein 4 gene (*Ltbp4*) decreased markedly at day 14 after bleomycin treatment (Supplemental Table S1). Ltbp4 regulates TGF-β1 bioavailability in pulmonary fibrosis.[39] Despite these insights into how changes in fibroblast gene expression can influence fibrogenesis, the significance of changes in the expression of many other genes remains elusive.

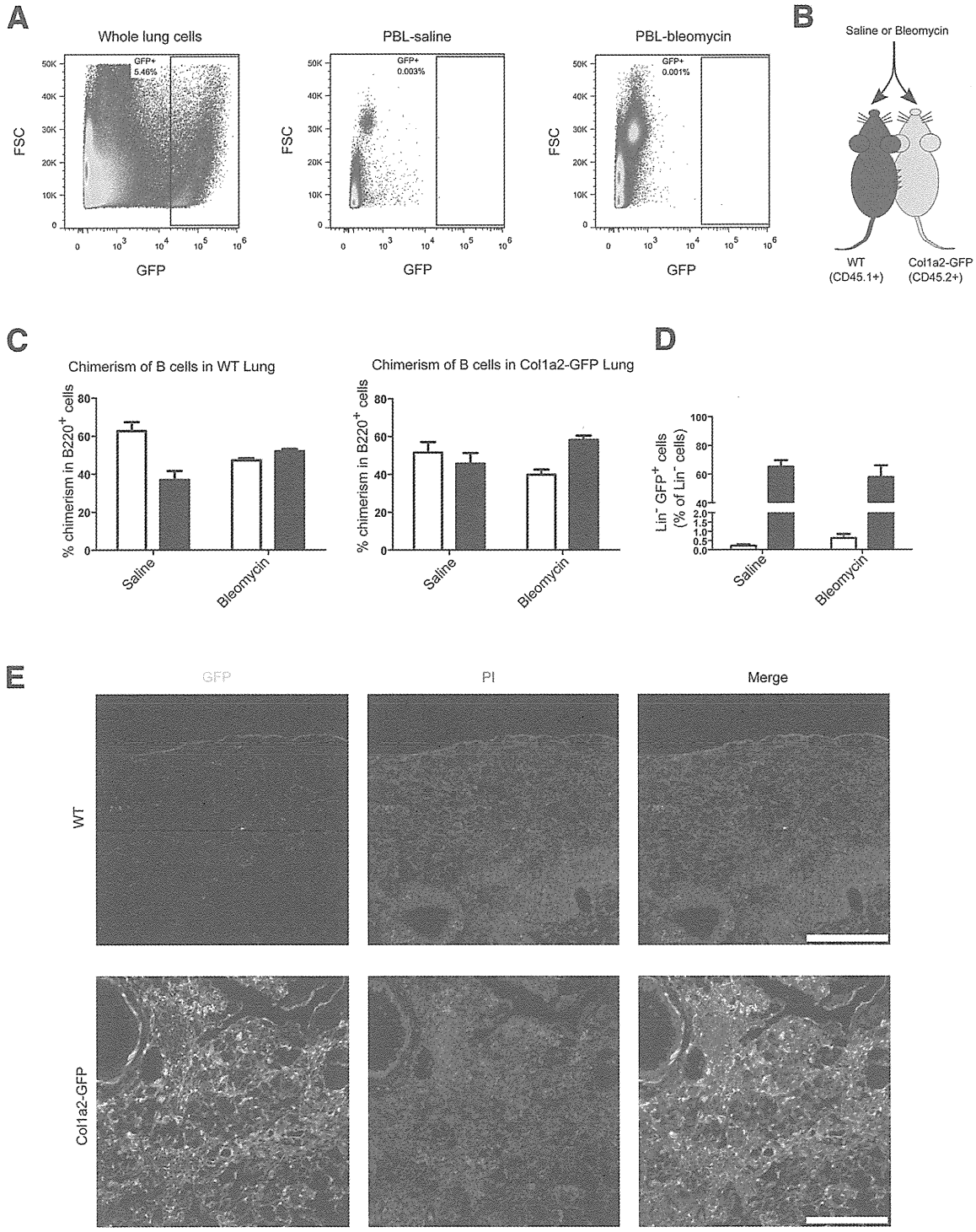

Figure 5 The contribution of bone marrow-derived cells to the lung GFP$^+$ fibroblast population. **A:** Whole-lung cells (saline treatment) and peripheral blood cells (saline or bleomycin treatment) were analyzed by flow cytometry at 14 days after treatment. Red plots are dense area, and blue plots are sparse area. **B:** Parabiotic pairs of WT (CD45.1$^+$) mice and Col1a2-GFP mice (CD45.2$^+$) were intratracheally instilled with bleomycin or saline. Each parabiotic pair received the same treatment. **C:** Chimerism of B cells (B220$^+$ cells) in the lungs of WT (white bars) or Col1a2-GFP (black bars) mice was determined from CD45.1 and CD45.2 expression. **D:** The proportion of GFP$^+$ cells in WT (white bars) and Col1a2-GFP (black bars) lungs was measured by flow cytometry. **E:** Representative lung sections of parabiotic WT and Col1a2-GFP mice stained for GFP and PI and imaged by confocal fluorescence microscopy. Data are expressed as means ± SEM (**C** and **D**). Scale bar = 250 μm. PBL, peripheral blood.

Previous studies have demonstrated roles for TGF-β, EGF, and IL-1β in pulmonary fibrosis.[5,40,41] By analyzing the gene expression profiles of fibroblasts with IPA software, we confirmed that these molecules worked directly as upstream gene regulators in fibroblasts (Supplemental Table S2). We also categorized up-regulated genes by molecular function, such as cytokine, chemotaxis, cell adhesion, and DNA binding (Supplemental Tables S3, S4, S5, and S6)

Table 1 The 40 Most up-Regulated Genes in GFP$^+$ Fibroblasts at 14 Days after Bleomycin Treatment

Symbol	Tags, no.		Fold change
	Saline	Bleomycin	
Spp1	57	12,155	213.2
Crlf1	1	212	212.0
Chl1	1	157	157.0
Cthrc1	1	97	97.0
Ereg	7	449	64.1
Anxa8	2	108	54.0
Lrg1	2	104	52.0
Hp	28	1,077	38.5
9930013L23Rik	4	103	25.8
Gjb3	4	98	24.5
C1qtnf6	13	298	22.9
Sdc1	6	136	22.7
Areg	3	66	22.0
Tnc	40	824	20.6
S100a4	116	2,060	17.8
Fst	36	568	15.8
Ildr2	6	86	14.3
Mcm6	6	74	12.3
Hspb7	9	106	11.8
Timp1	163	1,883	11.6
Slc7a2	8	88	11.0
Sfrp1	165	1,702	10.3
Fkbp5	10	95	9.5
Serpina3m	18	164	9.1
Rnf149	21	191	9.1
Fn1	1018	8,890	8.7
Chst11	10	87	8.7
Il11	8	66	8.3
*Nrep**	48	395	8.2
Cd109	16	118	7.4
1110038B12Rik	15	107	7.1
Slpi	23	164	7.1
Rgs16	25	176	7.0
Cyp26b1	11	75	6.8
Saa3	219	1,474	6.7
Nek6	12	78	6.5
Inhba	14	90	6.4
Col12a1	30	189	6.3
Col7a1	19	118	6.2
Wisp1	30	180	6.0

*Alias *D0H4S114*.

To assess the functional significance of changes in the gene expression profile of GFP$^+$ fibroblasts after bleomycin treatment, we used DAVID software to analyze which GO terms were enriched among genes that were up-regulated greater than threefold (Table 2).[21] Many of the up-regulated genes related to the ECM, suggesting that after bleomycin treatment the activated GFP$^+$ fibroblasts were involved in construction of ECM networks at fibrotic lesions. Genes related to the binding of extracellular components, such as glycosaminoglycan, were also up-regulated. We also used IPA software to quantify the specific changes in biological function associated with changes in gene expression in activated GFP$^+$ fibroblasts (Table 3). The IPA analysis yields an activation *z*-score that indicates the extent to which biological function is increased (positive values) or decreased (negative values). Genes that promote cell proliferation were up-regulated in activated GFP$^+$ fibroblasts, whereas functions linked to cell death, such as apoptosis and necrosis, had negative activation *z*-scores. These results indicate that activated GFP$^+$ fibroblasts are more resistant to cell death. Functions related to cell migration (including cell movement, invasion, and chemotaxis) were increased. Overall, these results mirror the assumed roles of fibroblasts in fibrogenesis; activated fibroblasts migrate to damaged sites and generate fibrotic legions by secreting ECM components. These data also support a central role for GFP$^+$ fibroblasts in bleomycin-induced fibrogenesis.

Identification of OPN as an Early Activation Marker of Lung Fibroblasts in Bleomycin-Induced Fibrosis

Because the OPN gene *Spp1* had both the highest fold change and the high read tag number in bleomycin-treated GFP$^+$ fibroblasts, we examined the possibility that OPN might serve as an activation marker for lung fibroblasts. Although T cells and macrophages are well-known sources of OPN, tissue cells may be important alternative sources of this protein.[42] We used qPCR to confirm *Spp1* expression levels in mRNA collected from sorted GFP$^+$ fibroblasts. *Spp1* mRNA levels were approximately 500 times higher in bleomycin-treated fibroblasts than in saline-treated fibroblasts (Figure 6A). To confirm protein expression, we cultured lung fibroblasts with BFA and stained them with an antibody against OPN before analysis by flow cytometry (Figure 6B). Of the Lin$^-$ bleomycin-treated GFP$^+$ fibroblasts, 9.0 $\pm$ 1.1% were OPN$^+$, compared with only 0.37 $\pm$ 0.07% of saline-treated GFP$^+$ fibroblasts (Figure 6C).

Table 2 Gene Ontology (GO) Terms That Were Enriched Amongst Genes That Were up-Regulated Greater than Threefold in GFP$^+$ Fibroblasts at 14 Days after Bleomycin Treatment

GO term	Genes, no.	*P* value
Extracellular region	40	2.58×10^{-14}
Extracellular region part	25	4.17×10^{-11}
Extracellular matrix part	11	3.04×10^{-10}
Proteinaceous extracellular matrix	16	5.03×10^{-10}
Extracellular matrix	16	8.70×10^{-10}
Collagen	5	5.60×10^{-06}
Cell adhesion	14	4.81×10^{-05}
Biological adhesion	14	4.90×10^{-05}
Glycosaminoglycan binding	7	7.71×10^{-05}
Basement membrane	6	1.01×10^{-04}
Pattern binding	7	1.46×10^{-04}
Polysaccharide binding	7	1.46×10^{-04}
Heparin binding	6	1.67×10^{-04}
Growth factor activity	7	2.48×10^{-04}
Extracellular structure organization	7	3.59×10^{-04}
Extracellular matrix organization	6	4.44×10^{-04}

Table 3 Changes in Biological Function Associated with Changes in Gene Expression in GFP^+ Fibroblasts at 14 Days after Bleomycin Treatment

Function annotation	*P* value	Predicted activation state	Activation *Z*-score
Proliferation of cells	1.19×10^{-42}	Increased	3.075
Necrosis	7.76×10^{-36}		−1.309
Cell death	2.45×10^{-35}		−1.146
Apoptosis	2.86×10^{-34}		−1.598
Cell movement	1.74×10^{-28}	Increased	3.756
Migration of cells	2.78×10^{-28}	Increased	3.179
Metabolism of protein	4.61×10^{-28}	Increased	2.429
Proliferation of fibroblasts	6.11×10^{-22}	Increased	2.54
Invasion of cells	1.96×10^{-20}	Increased	2.798
Proliferation of fibroblast cell lines	4.35×10^{-19}	Increased	2.526
Proliferation of connective tissue cells	2.36×10^{-18}	Increased	3.652
Migration of connective tissue cells	1.32×10^{-16}	Increased	2.843
Cell movement of connective tissue cells	2.77×10^{-16}	Increased	3.032
Migration of fibroblasts	7.95×10^{-16}	Increased	2.253
Cell movement of fibroblasts	5.39×10^{-15}	Increased	2.57
Cell spreading	1.08×10^{-13}	Increased	2.297
Adhesion of connective tissue cells	2.20×10^{-10}	Increased	2.849
Attachment of cells	1.65×10^{-08}	Increased	2.557
Chemotaxis	1.64×10^{-06}	Increased	2.317

Interestingly, most OPN^+ GFP^+ fibroblasts had an activated phenotype with high FSC and SSC (Figure 6B).

We also confirmed the expression of OPN in bleomycin-treated GFP^+ fibroblasts by immunofluorescence staining *in vitro* (Figure 6D) and *in vivo* (Figure 6E). OPN was detected in the cytoplasm around the nucleus, probably associated with the endoplasmic reticulum and intracellular vesicles (Figure 6D). *In vivo*, OPN^+ rounded leukocytes were detected in the alveolar air spaces, possibly representing alveolar macrophages.[42] OPN^+ GFP^+ fibroblasts existed at the boundaries between the alveolar air spaces and the fibrotic region where GFP^+ fibroblasts clustered (Figure 6E). In addition, some OPN^+ GFP^+ fibroblasts were detected adjacent to epithelium-denuded alveoli (Figure 6E). Some but not all OPN^+ GFP^+ fibroblasts coexpressed α-SMA, whereas GFP^+ fibroblasts clustering in fibrotic regions where the interstitium was thickened often expressed α-SMA but not OPN (Figure 6F). OPN^+ GFP^+ fibroblasts localized to places where alveolar structures still remained, but which appeared to be undergoing remodeling to form fibrotic regions (Figure 6F). Taken together, these results suggest that activated fibroblasts, especially those located at the edges of fibrotic regions, secrete OPN into the alveolar air spaces, resulting in an accumulation of OPN on the luminal surfaces of alveolar walls.

Discussion

The development of novel therapeutic strategies against pulmonary fibrosis requires a better understanding of fibroblast activation in the context of disease. We investigated the changes that occur in lung tissue cell populations, including fibroblast populations, after the induction of fibrosis. Unexpectedly, the number of fibroblasts present in the lungs did not increase, even at the peak of fibrosis, probably because proliferation and apoptosis were promoted concurrently in the fibrotic condition. Activated GFP^+ fibroblasts possessed a characteristic phenotype consisting of enlarged cell size, increased intracellular organelle complexity, and up-regulation of genes involved in fibrogenesis. Of these genes, the OPN-encoding gene was the most highly up-regulated. OPN appeared to be secreted into alveolar spaces by activated fibroblasts located at the edges of fibrotic regions.

Fibrotic regions are considered to develop as a consequence of fibroblast migration, proliferation, and subsequent accumulation. Some *in vitro* studies suggest that activated fibroblasts acquire increased proliferative capacity.[25,26,43] In addition, fibrosis and wound healing models have shown expansion of myofibroblasts *in vivo*.[44,45] On the other hand, fibroblast proliferation has been shown to be inhibited by polymerized collagen,[46] suggesting that proliferative regulation of fibroblasts *in vivo* may depend on the microenvironment. In our model, we observed BrdU uptake and clustering by GFP^+ fibroblasts. Although there is a possibility that repair of DNA damage could contribute in part to BrdU uptake, the increase in proliferative cells observed in Fucci mice is consistent with BrdU uptake by proliferating fibroblasts.

Comprehensive gene expression analysis revealed an up-regulation of proliferative genes but not apoptotic genes, whereas an increase of apoptotic fibroblasts was detected by flow cytometry. This difference may have arisen because SAGE was performed at day 14, rather than

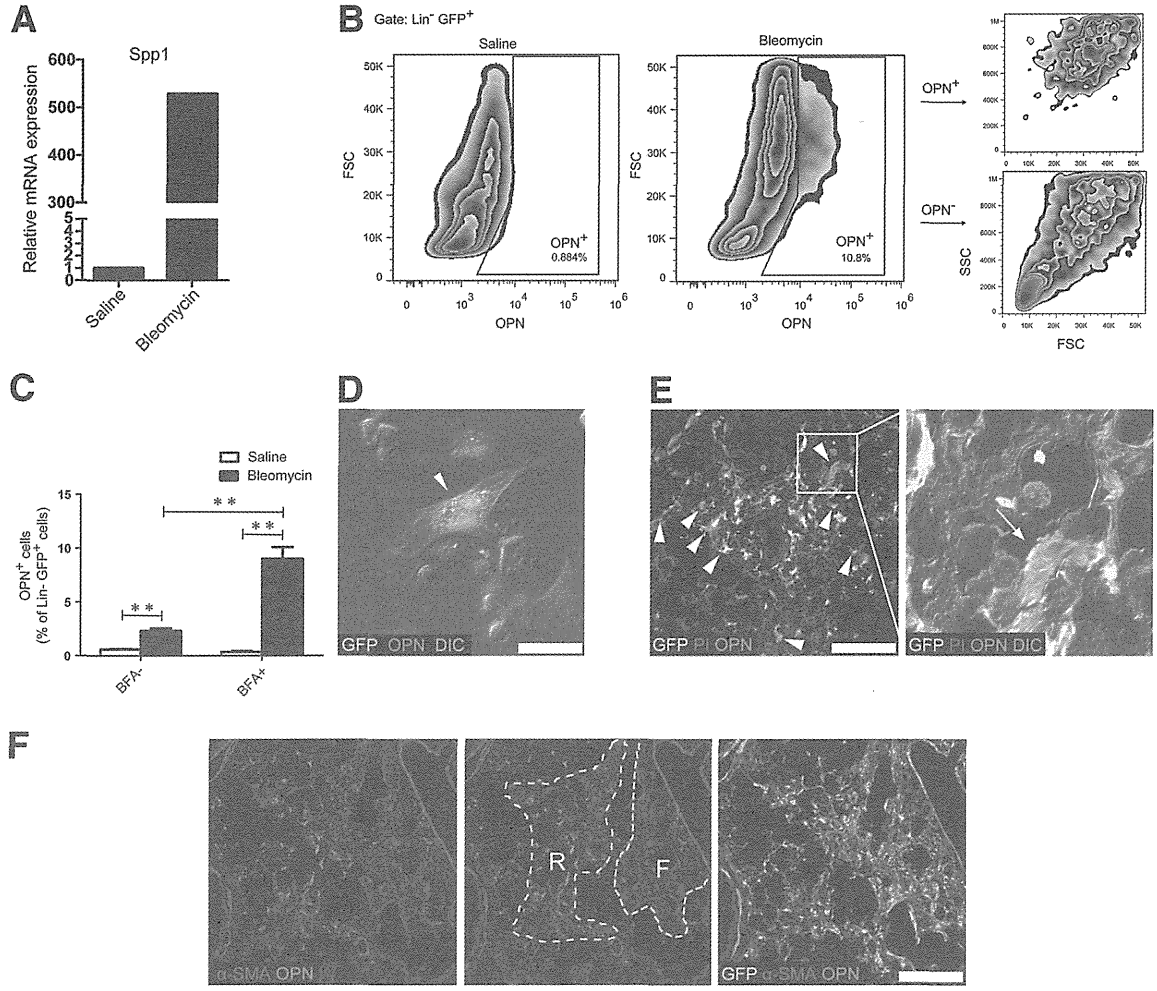

Figure 6 OPN is an activation marker of fibroblasts. **A:** mRNA isolated from sorted Lin$^-$ GFP$^+$ lung fibroblasts at 14 days after saline or bleomycin was analyzed by qPCR for *Spp1*. Template cDNA was pooled from the cells of three mice per group. **B:** Lung cells from Col1a2-GFP mice at 14 days after saline or bleomycin administration were cultured with BFA for 6 hours before staining for lineage markers and OPN (**left**). OPN$^+$ and OPN$^-$ Lin$^-$ GFP$^+$ fibroblasts from bleomycin-treated mice were plotted as FSC versus SSC (**right**). **C:** After 6 hour-culture of lung cells from saline or bleomycin-treated mice (day 14) with or without BFA, the proportion of Lin$^-$ GFP$^+$ cells that were OPN$^+$ was measured by flow cytometry. Data represent means ± SEM ($n = 4$). $^{**}P < 0.01$. **D:** Analysis by confocal microscopy of lung cells from Col1a2-GFP mice at 14 days after bleomycin administration. Cells were cultured *in vitro* with BFA for 6 hours before staining for OPN (red). OPN$^+$ GFP$^+$ cells are indicated by an **arrowhead**. **E:** Whole lungs from Col1a2-GFP mice at 14 days after bleomycin administration were cultured for 6 hours with BFA before sections were prepared and stained for OPN (red) and PI (blue). OPN$^+$ GFP$^+$ cells are indicated by **arrowheads** (**left**). The **boxed** region is shown at higher magnification at the **right**, highlighting an OPN$^+$ GFP$^+$ fibroblast (**arrow**) in an epithelium-denuded alveolus. **F:** Representative lung section from a Col1a2-GFP mouse at 14 days after bleomycin treatment, stained for α-SMA (blue) and OPN (red). Scale bars: 25 μm (**D**); 100 μm (**E**); 200 μm (**F**). F, fibrotic region; R, site of remodeling.

at day 7, when the peak of fibroblast apoptosis was observed. Also, because the proportion of apoptotic fibroblasts was very low (approximately 2%), the gene expression of apoptotic fibroblasts might have been negated by that of nonapoptotic fibroblasts. In such a case, the expansion of the population of GFP$^+$ fibroblasts revealed by their BrdU uptake might not have been sufficient to surpass the rate of cell death by apoptosis. Furthermore, long-term BrdU-uptake experiments revealed that fibroblasts can form fibrotic clusters without massive proliferation. These findings suggest that an absolute increase in fibroblast numbers is not necessarily critical to the pathogenesis of pulmonary fibrosis. Rather, it is fibroblast accumulation in clusters resulting from cell migration that is likely to be most important to the progression of fibrogenesis.

Immunohistochemical examination of fibrotic lungs revealed a massive increase in the number of GFP$^+$ fibroblast clusters in fibrotic regions. However, we do not believe that the increased density of GFP$^+$ fibroblasts that was observed with immunohistochemistry contradicts the flow-cytometric data showing that GFP$^+$ fibroblast numbers did not increase after bleomycin treatment. First, determining the proliferation of lung fibroblasts by histology is difficult, because fibrotic lung sections are filled with stroma (unlike normal lung sections, in which most of the area is made up of alveolar air spaces). Quantification of changes in tissue cell populations by flow cytometry after complete

digestion of whole lungs avoids such limitations. Second, in epithelium-denuded alveoli, fibroblasts encroach on the alveolar air space and there they secrete ECM components, resulting in coalescence of the alveolar walls.[47,48] Thus, the GFP^+ clusters observed in fibrotic regions are likely to be the result of fibroblast migration from surrounding alveolar walls into the alveolar air spaces. The up-regulation of genes associated with cell migration in GFP^+ fibroblasts supports this theory.

With the present study, we have identified OPN as an activation marker of lung fibroblasts during fibrosis. OPN is a matricellular protein that is implicated in various diseases, but that plays a different functional role from classical ECM proteins such as collagen or fibronectin.[49] Mori et al[50] found that knockdown of OPN decreased granulation tissue formation and scarring after skin injuries. Macrophage or mast cell-derived platelet-derived growth factor (PDGF) at the site of inflammation induced OPN expression in skin fibroblasts. Lenga et al[51] demonstrated that OPN is required for myofibroblast differentiation and activity in cardiac and skin fibroblasts. Macrophages, T cells, and epithelial cells are known sources of OPN in lung fibrosis. Although it has been reported previously that IL-1β induces OPN expression in lung fibroblasts *in vitro*,[52] the present study provides clear *in vivo* confirmation of OPN expression in lung fibroblasts during bleomycin-induced fibrosis. Other studies have suggested that epithelial cells, rather than fibroblasts, are the tissue cell source of OPN in pulmonary fibrosis.[35,42] A possible explanation for this discrepancy is that we treated the cells with BFA, and detection of the OPN protein in GFP^+ fibroblasts was greatly enhanced after BFA treatment (Figure 6C). Nevertheless, the relative contribution of various tissue cell populations, including fibroblasts, as sources of OPN in pulmonary fibrosis remains to be determined.

The finding that the OPN gene *Spp1* was highly up-regulated in GFP^+ fibroblasts after bleomycin treatment strongly suggests that OPN is involved in the pathogenesis of bleomycin-induced fibrosis. Previous studies have demonstrated that OPN enhances migration, invasion, and proliferation of lung fibroblasts.[35,53] Because OPN was abundant in alveolar air spaces, especially those near fibrotic regions, we suspect the involvement of OPN in the process of fibroblast migration to alveolar air spaces and in the formation of fibrotic foci through the coalescence of alveolar walls with ECM. In OPN-null mice, altered formation of fibrotic regions is observed, characterized by dilated distal air spaces.[42] Because the OPN gene *SPP1* is also one of the most highly up-regulated genes in human idiopathic pulmonary fibrosis,[35] understanding the role and mechanism action of OPN in the pathogenesis of fibrosis is likely to contribute to the development of novel therapies for this disease.

The comprehensive gene expression profile of freshly isolated fibroblasts suggested that activated fibroblasts became proliferative, resistant to cell death, mobile, and invasive. GO term enrichment demonstrated a role for these cells in ECM depositions, and flow cytometry and immunohistochemistry revealed expression of α-SMA in some GFP^+ fibroblasts. These findings suggest that, after bleomycin treatment, some GFP^+ resident fibroblasts differentiate into myofibroblasts and play a critical role in fibrogenesis. However, because the possibility cannot be excluded that other cell types such as epithelial cells acquire GFP expression and a fibroblast phenotype after bleomycin treatment, the findings in the present study should be confirmed by strict lineage tracing of fibroblasts. We demonstrated that GFP^+ fibroblasts in the lungs were not supplied from the circulation. In a study using the same Col1a2-GFP reporter mice, Higashiyama et al[54] found that limited but significant number of $CD45^+$ collagen type I–positive cells were recruited to skin in bleomycin-induced skin fibrosis. A possible explanation for the discrepancy between the present study and previous studies of fibrocytes is that we used parabiosis instead of bone marrow transplantation. Our present results clearly showed that circulating mesenchymal cells do not contribute significantly to fibroblast population in the lungs, and most of the fibroblasts in fibrotic regions are residential.

Interestingly, the localization of α-SMA–expressing fibroblasts and OPN-expressing fibroblasts differed. α-SMA–expressing fibroblasts were prominent within fibroblast clusters, whereas OPN-expressing fibroblasts were commonly located at the boundary of fibrotic regions and alveolar spaces. Thus, OPN expression and α-SMA expression may represent different stages of fibrogenesis. Currently, most fibrosis studies rely on α-SMA as a unique marker for myofibroblasts, based on the premise that myofibroblasts are the most important cell population in fibrogenesis. Given the various biological functions that OPN contributes to fibrogenesis, our findings suggest that OPN^+ collagen type I-producing fibroblasts represent a novel population of fibroblasts that play an important role in fibrogenesis, a role distinct from that of myofibroblasts.

In conclusion, we have revealed *in vivo* properties of fibroblasts during bleomycin-induced pulmonary fibrosis, showing their profibrotic signatures without changes in number. From the gene expression profile, the gene encoding OPN was identified as the most highly expressed gene in fibroblasts, with distinct localizations that are different from those of myofibroblasts, suggesting potential use of OPN as a novel activation marker of fibroblasts. Taken together, these findings provide useful insights toward further elucidation of the cellular and molecular mechanisms of pulmonary fibrosis.

Acknowledgments

We thank Dr. Atsushi Miyawaki and the RIKEN Bio-Resource Center cell bank for supplying FucciG1-#639 and FucciS/G2/M-#474 mice.

Supplemental Data

Supplemental material for this article can be found at *http://dx.doi.org/10.1016/j.ajpath.2013.06.005*.

References

1. Wynn TA, Ramalingam TR: Mechanisms of fibrosis: therapeutic translation for fibrotic disease. Nat Med 2012, 18:1028–1040
2. King TE Jr, Pardo A, Selman M: Idiopathic pulmonary fibrosis. Lancet 2011, 378:1949–1961
3. Wynn TA: Cellular and molecular mechanisms of fibrosis. J Pathol 2008, 214:199–210
4. Hinz B, Phan SH, Thannickal VJ, Galli A, Bochaton-Piallat ML, Gabbiani G: The myofibroblast. Am J Pathol 2007, 170:1807–1816
5. Wynn TA: Integrating mechanisms of pulmonary fibrosis. J Exp Med 2011, 208:1339–1350
6. Noble PW, Barkauskas CE, Jiang D: Pulmonary fibrosis: patterns and perpetrators. J Clin Invest 2012, 122:2756–2762
7. Kim KK, Wei Y, Szekeres C, Kugler MC, Wolters PJ, Hill ML, Frank JA, Brumwell AN, Wheeler SE, Kreidberg JA, Chapman HA: Epithelial cell alpha3beta1 integrin links beta-catenin and Smad signaling to promote myofibroblast formation and pulmonary fibrosis. J Clin Invest 2009, 119:213–224
8. Tanjore H, Xu XC, Polosukhin VV, Degryse AL, Li B, Han W, Sherrill TP, Plieth D, Neilson EG, Blackwell TS, Lawson WE: Contribution of epithelial-derived fibroblasts to bleomycin-induced lung fibrosis. Am J Respir Crit Care Med 2009, 180:657–665
9. Hoyles RK, Derrett-Smith EC, Khan K, Shiwen X, Howat SL, Wells AU, Abraham DJ, Denton CP: An essential role for resident fibroblasts in experimental lung fibrosis is defined by lineage-specific deletion of high-affinity type II transforming growth factor receptor. Am J Respir Crit Care Med 2010, 183:249–261
10. Rock JR, Barkauskas CE, Cronce MJ, Xue Y, Harris JR, Liang J, Noble PW, Hogan BLM: Multiple stromal populations contribute to pulmonary fibrosis without evidence for epithelial to mesenchymal transition. Proc Natl Acad Sci USA 2011, 108:E1475–E1483
11. Lin SL, Kisseleva T, Brenner DA, Duffield JS: Pericytes and perivascular fibroblasts are the primary source of collagen-producing cells in obstructive fibrosis of the kidney. Am J Pathol 2008, 173: 1617–1627
12. Göritz C, Dias DO, Tomilin N, Barbacid M, Shupliakov O, Frisén J: A pericyte origin of spinal cord scar tissue. Science 2011, 333: 238–242
13. Herzog EL, Brody AR, Colby TV, Mason R, Williams MC: Knowns and unknowns of the alveolus. Proc Am Thorac Soc 2008, 5:778–782
14. Kunz-Schughart LA, Wenninger S, Neumeier T, Seidl P, Knuechel R: Three-dimensional tissue structure affects sensitivity of fibroblasts to TGF-beta 1. Am J Physiol Cell Physiol 2003, 284:C209–C219
15. De Val S, Ponticos M, Antoniv TT, Wells DJ, Abraham D, Partridge T, Bou-Gharios G: Identification of the key regions within the mouse pro-alpha 2(I) collagen gene far-upstream enhancer. J Biol Chem 2001, 277:9286–9292
16. Higashiyama R, Moro T, Nakao S, Mikami K, Fukumitsu H, Ueda Y, Ikeda K, Adachi E, Bou-Gharios G, Okazaki I, Inagaki Y: Negligible contribution of bone marrow-derived cells to collagen production during hepatic fibrogenesis in mice. Gastroenterology 2009, 137: 1459–1466
17. Tomura M, Mori YS, Watanabe R, Tanaka M, Miyawaki A, Kanagawa O: Time-lapse observation of cellular function with fluorescent probe reveals novel CTL-target cell interactions. Int Immunol 2009, 21:1145–1150
18. Foster WM, Walters DM, Longphre M, Macri K, Miller LM: Methodology for the measurement of mucociliary function in the mouse by scintigraphy. J Appl Physiol 2001, 90:1111–1117
19. Shimbori C, Shiota N, Okunishi H: Involvement of leukotrienes in the pathogenesis of silica-induced pulmonary fibrosis in mice [Erratum appeared in Exp Lung Res 2010, 36:440]. Exp Lung Res 2010, 36: 292–301
20. Fujita M, Shannon JM, Irvin CG, Fagan KA, Cool C, Augustin A, Mason RJ: Overexpression of tumor necrosis factor-alpha produces an increase in lung volumes and pulmonary hypertension. Am J Physiol Lung Cell Mol Physiol 2001, 280:L39–L49
21. Huang DW, Sherman BT, Lempicki RA: Systematic and integrative analysis of large gene lists using DAVID bioinformatics resources. Nat Protoc 2008, 4:44–57
22. Kapanci Y, Ribaux C, Chaponnier C, Gabbiani G: Cytoskeletal features of alveolar myofibroblasts and pericytes in normal human and rat lung. J Histochem Cytochem 1992, 40:1955–1963
23. Fukuda Y, Ferrans VJ, Schoenberger CI, Rennard SI, Crystal RG: Patterns of pulmonary structural remodeling after experimental paraquat toxicity. The morphogenesis of intraalveolar fibrosis. Am J Pathol 1985, 118:452–475
24. Kawamoto M, Fukuda Y: Cell proliferation during the process of bleomycin-induced pulmonary fibrosis in rats. Acta Pathol Jpn 1990, 40:227–238
25. Moseley PL, Hemken C, Hunninghake GW: Augmentation of fibroblast proliferation by bleomycin. J Clin Invest 1986, 78:1150–1154
26. Mio T, Nagai S, Kitaichi M, Kawatani A, Izumi T: Proliferative characteristics of fibroblast lines derived from open lung biopsy specimens of patients with IPF (UIP). Chest 1992, 102:832–837
27. Messier EM, Mason RJ, Kosmider B: Efficient and rapid isolation and purification of mouse alveolar type II epithelial cells. Exp Lung Res 2012, 38:363–373
28. Mouratis MA, Aidinis V: Modeling pulmonary fibrosis with bleomycin. Curr Opin Pulm Med 2011, 17:355–361
29. Zhang K, Rekhter MD, Gordon D, Phan SH: Myofibroblasts and their role in lung collagen gene expression during pulmonary fibrosis. A combined immunohistochemical and in situ hybridization study. Am J Pathol 1994, 145:114–125
30. Takemoto K: Spatio-temporal activation of caspase revealed by indicator that is insensitive to environmental effects. J Cell Biol 2003, 160:235–243
31. Nagai T, Miyawaki A: A high-throughput method for development of FRET-based indicators for proteolysis. Biochem Biophys Res Commun 2004, 319:72–77
32. Sakaue-Sawano A, Kurokawa H, Morimura T, Hanyu A, Hama H, Osawa H, Kashiwagi S, Fukami K, Miyata T, Miyoshi H, Imamura T, Ogawa M, Masai H, Miyawaki A: Visualizing spatiotemporal dynamics of multicellular cell-cycle progression. Cell 2008, 132:487–498
33. Phillips RJ, Burdick MD, Hong K, Lutz MA, Murray LA, Xue YY, Belperio JA, Keane MP, Strieter RM: Circulating fibrocytes traffic to the lungs in response to CXCL12 and mediate fibrosis. J Clin Invest 2004, 114:438–446
34. Hashimoto N: Bone marrow-derived progenitor cells in pulmonary fibrosis. J Clin Invest 2004, 113:243–252
35. Pardo A, Gibson K, Cisneros J, Richards TJ, Yang Y, Becerril C, Yousem S, Herrera I, Ruiz V, Selman M, Kaminski N: Up-regulation and profibrotic role of osteopontin in human idiopathic pulmonary fibrosis. PLoS Med 2005, 2:e251
36. Kaminski N, Allard JD, Pittet JF, Zuo F, Griffiths MJ, Morris D, Huang X, Sheppard D, Heller RA: Global analysis of gene expression in pulmonary fibrosis reveals distinct programs regulating lung inflammation and fibrosis. Proc Natl Acad Sci USA 2000, 97: 1778–1783
37. Kass DJ, Yu G, Loh KS, Savir A, Borczuk A, Kahloon R, Juan-Guardela B, Deiuliis G, Tedrow J, Choi J, Richards T, Kaminski N, Greenberg SM: Cytokine-like factor 1 gene expression is enriched in idiopathic pulmonary fibrosis and drives the accumulation of CD4+ T cells in murine lungs. Am J Pathol 2012, 180:1963–1978
38. Oikonomou N, Thanasopoulou A, Tzouvelekis A, Harokopos V, Paparountas T, Nikitopoulou I, Witke W, Karameris A, Kotanidou A,

Bouros D, Aidinis V: Gelsolin expression is necessary for the development of modelled pulmonary inflammation and fibrosis. Thorax 2009, 64:467–475
39. Zhou Y, Koli K, Hagood JS, Miao M, Mavalli M, Rifkin DB, Murphy-Ullrich JE: Latent transforming growth factor-β-binding protein-4 regulates transforming growth factor-β1 bioavailability for activation by fibrogenic lung fibroblasts in response to bleomycin. Am J Pathol 2009, 174:21–33
40. Ishii Y: Gefitinib prevents bleomycin-induced lung fibrosis in mice. Am J Respir Crit Care Med 2006, 174:550–556
41. Wilson MS, Madala SK, Ramalingam TR, Gochuico BR, Rosas IO, Cheever AW, Wynn TA: Bleomycin and IL-1-mediated pulmonary fibrosis is IL-17A dependent. J Exp Med 2010, 207:535–552
42. Berman JS: Altered bleomycin-induced lung fibrosis in osteopontin-deficient mice. Am J Physiol Lung Cell Mol Physiol 2004, 286: L1311–L1318
43. Ramos C, Montaño M, García-Alvarez J, Ruiz V, Uhal BD, Selman M, Pardo A: Fibroblasts from idiopathic pulmonary fibrosis and normal lungs differ in growth rate, apoptosis, and tissue inhibitor of metalloproteinases expression. Am J Respir Cell Mol Biol 2001, 24:591–598
44. Humphreys BD, Lin SL, Kobayashi A, Hudson TE, Nowlin BT, Bonventre JV, Valerius MT, McMahon AP, Duffield JS: Fate tracing reveals the pericyte and not epithelial origin of myofibroblasts in kidney fibrosis. Am J Pathol 2010, 176:85–97
45. Virag JI, Murry CE: Myofibroblast and endothelial cell proliferation during murine myocardial infarct repair. Am J Pathol 2003, 163: 2433–2440
46. Xia H, Nho R, Kleidon J, Kahm J, Henke CA: Polymerized collagen inhibits fibroblast proliferation via a mechanism involving the formation of a beta1 integrin-protein phosphatase 2A-tuberous sclerosis complex 2 complex that suppresses S6K1 activity. J Biol Chem 2008, 283:20350–20360
47. Noble PW: Back to the future: historical perspective on the pathogenesis of idiopathic pulmonary fibrosis. Am J Respir Cell Mol Biol 2005, 33:113–120
48. Myers J, Katzenstein A: Epithelial necrosis and alveolar collapse in the pathogenesis of usual interstitial pneumonia. Chest 1988, 94: 1309–1311
49. Uede T: Osteopontin, intrinsic tissue regulator of intractable inflammatory diseases. Pathol Int 2011, 61:265–280
50. Mori R, Shaw TJ, Martin P: Molecular mechanisms linking wound inflammation and fibrosis: knockdown of osteopontin leads to rapid repair and reduced scarring. J Exp Med 2008, 205:43–51
51. Lenga Y, Koh A, Perera AS, McCulloch CA, Sodek J, Zohar R: Osteopontin expression is required for myofibroblast differentiation. Circ Res 2008, 102:319–327
52. Serlin DM, Kuang PP, Subramanian M, O'Regan A, Li X, Berman JS, Goldstein RH: Interleukin-1β induces osteopontin expression in pulmonary fibroblasts. J Cell Biochem 2006, 97:519–529
53. Anwar A, Li M, Frid MG, Kumar B, Gerasimovskaya EV, Riddle SR, McKeon BA, Thukaram R, Meyrick BO, Fini MA, Stenmark KR: Osteopontin is an endogenous modulator of the constitutively activated phenotype of pulmonary adventitial fibroblasts in hypoxic pulmonary hypertension. Am J Physiol Lung Cell Mol Physiol 2012, 303:L1–L11
54. Higashiyama R, Nakao S, Shibusawa Y, Ishikawa O, Moro T, Mikami K, Fukumitsu H, Ueda Y, Minakawa K, Tabata Y, Bou-Gharios G, Inagaki Y: Differential contribution of dermal resident and bone marrow–derived cells to collagen production during wound healing and fibrogenesis in mice. J Invest Dermatol 2011, 131: 529–536

最近の研究

マウス皮膚創傷治癒モデルにおける筋膜由来線維芽細胞と希少コラーゲンのはたらき

住吉秀明*
稲垣豊**

1．はじめに

コラーゲンは動物の細胞外マトリックス（Extracellular Matrix：以下ECM）の主成分を成す線維性構造タンパク質である．多細胞生物はECMの存在なしに成立せず，私はその重要性を表現する際にレンガ建築のレンガ（細胞）とセメント（ECM）に例えたりしている．コラーゲンは動物性タンパク質の3割を占める最も豊富な成分であるとともに，グリシン，プロリンの含有量が高く，自身のコラーゲンを合成するためにおいても良質の動物性タンパク質である．そのイメージは健康食品や美容，アンチエイジングの話題を中心とした健康に良い善玉として一般的にもよく浸透している．それに対し，我々は医学部の研究テーマにおいて肝硬変をはじめとする組織・臓器線維症を治療する研究を行っており，そこではコラーゲンは線維化を引き起こす悪玉として，如何に合成・蓄積されないようにするかを研究している．コラーゲンの総量は精妙に調節されなければならないが，慢性炎症等の病的要因により生合成と分解のバランスが崩れて過多に蓄積することにより，組織・臓器の機能を損なうのが線維症の実体である．コラーゲンはどの組織にも存在するため，線維化病変は肺線維症，腎硬化症，ケロイドの形成，手術後の癒着など，多領域にわたって重篤な疾患が存在し，これから解決されなければならない医療上の課題となっている．

本稿では傷病により誘導されたコラーゲンが如何にして構築・形成されていくかの過程をリアルタイムで観察する目的で，マウス皮膚創傷治癒をモデルとし，活性化線維芽細胞の動員，発現誘導されるコラーゲン遺伝子群の型別解析，コラーゲン線維束の形成過程を分子会合レベルで解析した例を示す．それらの結果，動員される線維芽細胞は真皮のものではなく，筋膜由来の静止線維細胞が活性化して動員されたもので，形成されるコラーゲン線維の性質も異なるということ，この細胞は希少コラーゲン分子種であるV型コラーゲンα3鎖（以下α3（V）と表記）を特異的に発現すること，このα3（V）はコラーゲン線維の会合・集束を阻害することで，その過剰形成を自ら抑制し，また皮膚組織と筋膜組織の癒着の防止に働いていることが新たに見出された．コラーゲンは多細胞組織に必要とされる生育環境の土台であり，線維の産生は細胞が生育環境を造りだそうとする自己防衛反応であるが，これは線維構築を制御し，安定終息させる生体側の仕組みであると思われ，その機序の解明が期待される．この稿は本会誌の中で，少し側面の異なる話となるが読者にとって，新たな興味となれれば幸いである．

2．実験の背景

コラーゲンは結合組織の支持体として働いているが，同時にそれは単なる支持体ではなく，他のECM分子と共に細胞の外部生育環境を構成し“細胞のゆりかご”として機能している．細胞に適した“足場”を提供し，また情報伝達の媒体となり，細胞に適する居場所や方向性の情報を与え，細胞と共に組織の形態を決定していく．このような能動的な役割を有しており，必ずしもセメントのような“接着させる物質”では無い．本来，細胞とECMは組織形態維持と機能発現に不可欠な要素であるが，その比率と正常な配位関係が失われれば，お互い足を引っ張り合う様に機能不全に陥る．特に肝臓は大きな再生能力を有しているにもかかわらず，肝硬変になると線維化によって肝再生が障害される．肝線維症の治療と肝細胞の再生医療は同じ事象の表裏であり，抗線維化治療法の開発の持つ意味は大き

*Hideaki Sumiyoshi：東海大学医学部再生医療科学，同総合医学研究所特任講師，**Yutaka Inagaki：東海大学医学部再生医療科学，同総合医学研究所教授，〒259-1193 神奈川県伊勢原市下糟屋143，TEL 0463(93)1121，内線3068